Population Kinetics of a Repetitively-Pulsed Nanosecond Discharge

by

Benjamin T. Yee

A dissertation submitted in partial fulfillment
of the requirements for the degree of
Doctor of Philosophy
(Nuclear Engineering & Radiological Sciences)
in the University of Michigan
2013

Doctoral Committee:

Associate Professor John E. Foster, Chair
Doctor Edward V. Barnat, Sandia National Laboratories
Doctor Isaiah M. Blankson, National Aeronautics and Space Administration
Professor Augustus Evrard
Professor Mark J. Kushner

2013

I would like to dedicate this dissertation to someone else.

A C K N O W L E D G M E N T S

Who is this?

Preface

This is a dissertation about something; I really hope it's good.

TABLE OF CONTENTS

LIST OF FIGURES

LIST OF TABLES

LIST OF APPENDICES

LIST OF ABBREVIATIONS

RPND repetitively-pulsed nanosecond discharge

APP atmospheric-pressure plasma

EEDF electron energy distribution function

FIW fast ionization wave

LCIF laser collision-induced fluorescence

MHD magnetohydrodynamic

FWHM full-width half maximum

FID fast ionization dynistor

MIPT Moscow Institute of Physics and Technology

CCD charge-coupled device

PTFE polytetrafluoroethylene

CHAPTER 1

Introduction

1.1 Overview

1.1.1 Motivation

Plasmas, commonly called the fourth state of matter, are a gas where a significant fraction of the neutral atoms or molecules have been split into pairs of electrons and positive ions. Initially, a curiosity of the laboratory, they have become a critical part of every day life. The electrically charged nature of plasmas makes them a practical means by which to convert electrical energy into electromagnetic, chemical, kinetic, or even nuclear energy. From an applications perspective, they are indisposable in lighting, semiconductor manufacturing, plastic processing, and space propulsion. On a more broad scale, virtually all observable light in the universe is the result of a plasma in some form or another [4].

Some exceptions aside, only three things are required to create a plasma: a gas, an energy source, and a means of transferring the energy to the gas. In man-made applications, the energy source is typically electricity, and the simplest transfer mechanism is via two electrodes placed on either side of the gas. The application of a potential difference to these electrodes produces an electric field as seen in figure 1.1. The field accelerates a single seed electron in the gas (often created by background cosmic radiation) until it collides with a neutral particle. The electron, having acquired a sufficient amount of energy, liberates a second electron loose from the particle, leaving behind a relatively heavy and immobile

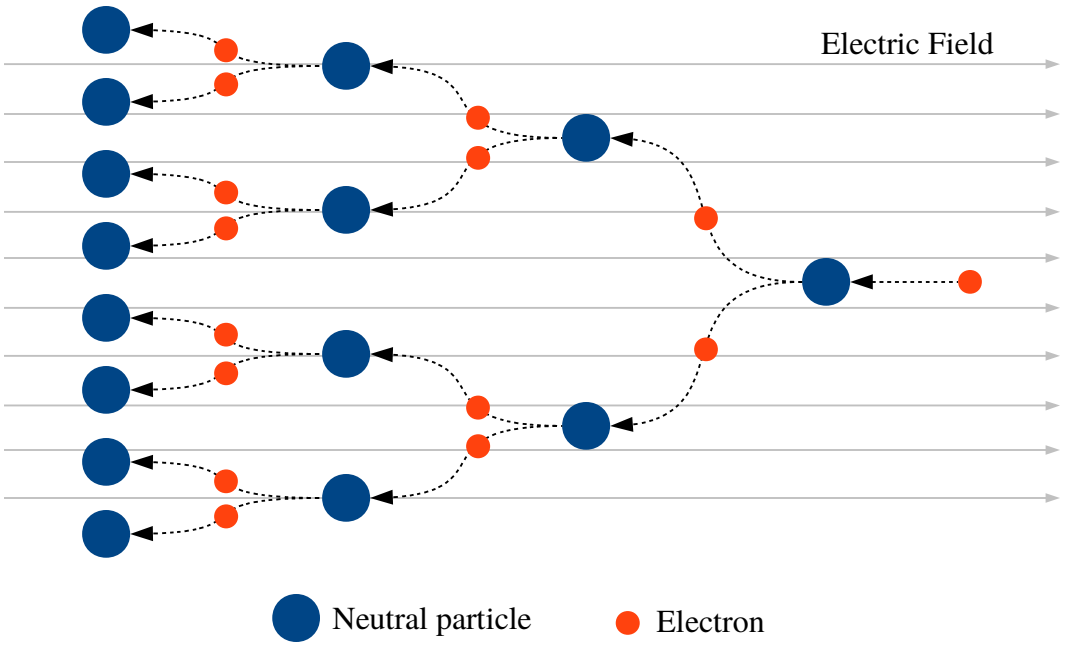

Figure 1.1: A simplified depiction of the avalanche breakdown process in a gas.

ion. Subsequently, both the first and second electron are now accelerated by the electric field. Again, they collide with two more neutral atoms, creating two new electrons. As long as the electric field persists, the number of electron and ion pairs increases exponentially. This process is generally referred to as an avalanche.

Eventually, the production of ions and electrons in the gap balances out with the rate at which they leave the system, whether by collection at the electrodes or some other process. The resulting ionized gas may be referred to as a plasma if it meets certain criteria. Simply put, there must be a high enough density and number of charged particles for their electromagnetic interaction to dominate over random collisions with neutral gas particles.

Despite this relatively simple recipe, the physical characteristics can vary greatly depending on what gas is used, what pressure it is at, what voltage is used, whether the electricity is applied constantly or varied over time, what kind of electrodes are used, etc. As a result, man-made plasmas are generally produced under very specific conditions. For example, a plasma etcher used in semiconductor manufacturing may need to operate oper-

ate at pressures that are one-thousandth of atmospheric pressure with ultra-pure (99.999%) gases [5].

Plasmas like those which occur in plasma etchers, feature ions and neutral gas particles with temperatures that are below 1,000 K, or roughly 1,340° F. Though this temperature is relatively high compared to room temperature, it is well below the temperature of the electrons which may be in excess of 20,000 K. Plasmas which exhibit this disparity in temperatures are often called nonequilibrium or "low-temperature" plasmas.

Conversely, there exists another class of plasmas where the electrons, ions, and neutral particles are all at the same temperature. These are called thermal plasmas. Generally speaking, the closer the gas pressure is to atmosphere, the more thermal a plasma is owing to the rapid increase in the frequency of collisions between neutral and charged particles [6]. Additionally, the temperatures in a thermal plasma can be quite high and, in many cases, can easily melt all metals assuming that the total energy content of the plasma is high enough. For example, the arc of an arc welder is a thermal plasma. Similar high temperature plasmas, have a number of other applications which include a variety of high-intensity lamps, metal cutting, and surface coating.

There are, however, a number of applications which would benefit from operation at higher pressures, but with low-temperature ions and neutrals so as to avoid heat damage. This has spurred a substantial amount of research on nonequilibrium atmospheric-pressure plasmas (APPS) in recent years [7]. Ideally, such a plasma could be generated at or near atmospheric pressure with hot electrons, but minimal heating of surrounding gas. Though this field of research is still relatively young, it has produced a variety of new plasmas and capabilities. One of the more ubiquitous examples is use of plasmas to process the surface of plastics so that ink can adhere. Separately, nonequilibrium APPS are the technology which drives plasma televisions [8].

As mentioned, these applications promise to be the first of many for such plasmas. More recently, there have been innovative proposals to use these plasmas in water purification [9],

wound sterilization [10], improved combustion engines [11], nanoparticle production [12], and more. However, each situation has its own challenges when it comes to the design and development of a plasma source, particularly at these elevated pressures. Particularly problematic is the tendency of APPs to develop instabilities which can cause them to rapidly transition to thermal plasmas in a matter of nanoseconds.

There exist a few ways of getting around these instabilities. One example is the dielectric-barrier discharge which passively regulates the amount of power which can be deposited into the plasma [13]. Another example includes split-ring resonators which use natural feedback mechanisms to damp out potential instabilities [14]. The technique considered here, referred to as the repetitively-pulsed nanosecond discharge, or RPND, uses high voltage pulses which are so short that the instability does not have time to develop [15]. The RPND is a nonequilibrium plasma which can operate at pressures ranging from approximately 10^{-3}–1 atmospheres [16]. At atmospheric pressure the RPND can produce a uniform plasma in volumes on the order of 10 mL [17]. As the pressure is reduced, the plasma volume can reach the order of liters [18].

The importance of large-area, uniform, high-pressure plasmas such as the RPND was highlighted in the National Academies' most recent decadal survey of plasma science [4]. However, there is still much that is not know about such plasmas. From the same survey, it is said that "the full promise of APPs will be known only if they can be understood and managed based on fundamental scientific principles at two extremes–the nanoscopic kinetic level, where selective chemistry occurs, and the global stability level." It is this challenge, specifically the investigation of the nanoscopic kinetic level, which drives the research presented here.

1.1.2 History

Historically, the study of low-temperature APPs has been almost indistinguishable from the study of plasmas as a whole. However, this was not necessarily a matter of reasoned choice.

Plasma generation at atmospheric-pressure obviates the need for an effective vacuum pump. Additionally, prior to the creation of large battery banks, early sources of electrical energy had relatively small capacities. This precluded the generation of thermal atmospheric plasmas which required large amounts of energy.

Indeed, the requirements for a low-temperature APP are sufficiently rudimentary that the first man-made one (and likely the first man-made plasma), was probably a spark generated by rubbing fur against amber. This is commonly attributed to Thales of Milêtus from around 600 B.C. Following Thales, electrical sparks came to intrigue many scientists including Gottfried Liebniz, Benjamin Franklin, and Charles Wheatstone. By the mid-1800s, Plücker, Geißler, and Hittorf began some of the first work on low-pressure plasmas though it was Crookes who would later identify plasma as a separate state of matter. Later, J.J. Thomson's discovery of the electron and discretized charge in 1897 marked the beginning of modern plasma research.

By this time, the necessary tools and techniques existed to create steady plasmas in pure, rarified gases. The behaviors of which were dominated by the motion and interaction of the charged electrons and ions. Critically, the effects of the neutral particles were negligible, thus isolating the electrical properties of the plasma. These carefully controlled systems were ideal for basic studies of plasma behavior and were used to great effect by individuals such as Lewi Tonks and Irving Langmuir [19]. In fact, many modern concepts in plasma physics can be traced back to their work.

In contrast, the pulsed APPS, characteristic of the earliest man-made plasmas [20], were easy to create, but notoriously difficult to work with. It could take them only a few nanoseconds to form, and less than a millisecond to decay away. For many years, there were simply no instruments capable of taking measurements this quickly. Furthermore, the neutral particles which were of no consequence in the low-pressure plasmas, could not be ignored. The neutral particles were present in such quantities that they could confound or obscure otherwise simple measurements.

As a consequence, there is still a great deal that is not known about about pulsed APPS, particularly lightning, streamers, and a type of plasma which Thomson referred to as a "luminous front." By the 1970s, this latter plasma had come to be called the fast ionization wave, or FIW [16]. It was generated by a single voltage pulse lasting around 100 nanoseconds and peaking at 10s or 100s of kilovolts. For the right pressure and gas, the FIW could fill volumes of nearly 40 L with a relatively uniform plasma, but with little heating of the gas.

These properties were attractive for a number of uses, but the FIW faced a number of implementation-related challenges. The switches used to trigger the FIW could only operate up to 100 times each second [21]. Unfortunately, the lifetime of a plasma at elevated pressures is relatively short, and the plasma generated by the FIW would decay away quickly after each pulse. This meant that the FIW-generated plasma had a relatively low duty cycle; the ratio of the time the plasma spends on to the time it spends off. This was disadvantageous for plasma-processing applications where low duty cycles are equivalent to long processing times. The low duty cycle also necessitated so-called preionization of the gas with UV lamps or a secondary plasma generator, adding to the cost and complexity of the system [22]. Finally, the pulse generators used for FIWs were not considered reliable enough for long operational lifetimes.

Recent advances in solid-state switching technology has largely solved these issues. At present, switches exist which can reliably operate 100,00 times a second; sufficiently fast that the plasma duty cycle approaches 100% [23]. This has the additional benefit of obviating the need for a preionization stage, as a sufficient number of electrons persist between pulses. The discharge produced by the use of these new switches is what we refer to as the RPND.

1.1.3 Questions

The large pedigree of pulsed plasma research belies the fact that they are still not well-understood. This remains especially true for RPNDS which present significant experimental

challenges. A major component of this has to do with the time scales associated with the RPND. The formation of a RPND often requires no more than a few nanoseconds. Very sensitive equipment is required in order to measure changes which occur during this period. Unfortunately, such equipment is particularly susceptible to the broadband electronic noise generated by both real and displacement currents of the fast pulses. There is a plethora of other problems that can be traced back to topic of timing. For example, the length and insulators of detector cables can introduce substantial delays, and must be considered in order to synchronize different measurements.

Consequently, the majority of RPND studies focus on measurements after the discharge has occurred, when changes happen at a much slower rate. A great deal of information is available for this period of time, including chemical compositions, atomic densities, electron densities, gas temperatures, and more. While undoubtedly important, these measurements provide limited insight on what is happening *while* the plasma is forming. It is natural, then, to ask, what are the RPND plasma properties during formation?

Additionally, most studies have used a limited range of gases: oxygen, nitrogen, air, hydrogen, or some mixture thereof. The choice of these gases is deliberate and reflects specific applications in combustion and aerospace. However, the use of rare gases (such as helium) and rare gas mixtures has become popular because they provide for a wider range of stable operating conditions. Notably, it has been found that the unique internal electronic structure of rare gases can produce very different discharges. Given this, there is the question of how rare gas RPNDs compare to more conventional ones.

Finally, the persistence of the plasma between pulses makes the development of a RPND very different from a FIW.

Finally, though the RPND and FIW are qualitatively similar, there are some fundamental differences between the two. These largely stem from the persistence of the plasma between pulses. It is this plasma which guarantees uniform breakdown in the case of RPND, while the FIW is largely dependent on very high energy electrons. At the same time, if the plasma is too

dense at the beginning of the voltage pulse, it can limit the final density of the electrons and excited atoms. Because plasma-induced chemistry is a product of these particles, this pre-pulse plasma plays a decisive role in the number of reactions a RPND can produce. Therefore, one must ask how the properties of a RPND compare to those of a FIW and how they vary with the operating conditions.

1.1.4 Approach

The dissertation presented here represents efforts to either answer or provide a foundation to answer these questions. In order to develop the appropriate context for this work, the next section will be a comprehensive review of the RPND literature. It begins with the first reported pulsed APPs and concludes with contemporary studies.

The following two chapters set the basis for the experimental and numerical studies. Chapter 2 presents the theory necessary to understand RPNDs including streamer discharges, atomic spectroscopy, and collision processes. Subsequently, chapter 3 describes the design of the helium RPND discharge apparatus used for the experimental studies and as the basis for the simulations. Also included in this chapter are several measurements of the basic discharge properties.

Chapters 4 through 6 provide more detailed measurements and analysis of the RPND dynamics. In chapter 4, the measurements of the helium metastables in a RPND are presented and analyzed as a function of pressure an axial location in the discharge apparatus. Chapter 5 presents and analyzes similar measurements of the spontaneous plasma emissions. Finally, chapter 6 discusses the development of a global model for a helium plasma and its use with the experimental data to infer the plasma properties of the RPND. The dissertation concludes with a summary of the results and suggestions for further avenues of research.

1.2 Literature Review

RPNDS are only a recent invention which resulted from advances in fast-switching semiconductors. However, the physics of their formation is related to a much more broad category of plasmas which includes lightning, streamers, and even some transient phenomena in DC glows [24]. These plasmas are unique in that their spatial structure develops at speeds much faster than can be accounted for by the conventional Townsend mechanism. Loeb refers to this phenomena as "ionizing waves of potential gradient." [1].

1.2.1 Early History of Pulsed Discharges

In 1835 (as reported by Thomson [1]), Charles Wheatstone attempted to measure what he thought to be the speed of electricity in a six-foot long discharge tube of unspecified pressure [25]. It is now known that he was actually measuring the speed with which a plasma formed between the two electrodes. He accomplished this by the use of a rotating mirror which allowed him to see images of two sections of the tube, slightly displaced. The displacement between the images was proportional to the speed with which the plasma traveled between them. Wheatsone estimated this speed to be at least 8×10^7 cm/s.

Interestingly, von Zahn later noted that this was *not* the speed of the emitting particles [26]. The visible light did cross the gap at an appreciable speed, but there was no detectable Doppler shift in the light emitted parallel to the propagation. As a result, it was concluded the light-emitting particles could not be traveling at the same speed as the light.

Later, Thomson revisited this work with an improved apparatus [1]. This included a tube that was now 15 m in length and five mm in diameter, as seen in figure 1.2. Also using the rotating mirror apparatus, Thomson was able to greatly improve on the estimates of Wheatstone. He estimated that the so-called "luminous front" had a speed that was more

[1] It should be noted that the phrase wave does not indicate any kind of periodic motion or spatial arrangement. Simply put, it describes a boundary which separates ionized and unionized gas which travels from one electrode to another.

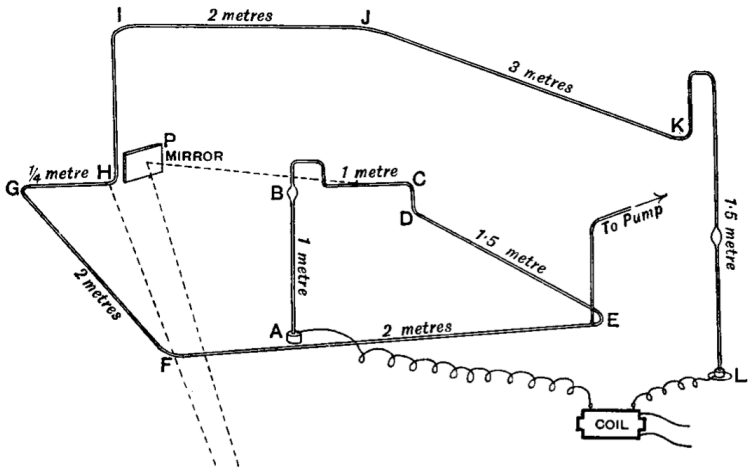

Figure 1.2: A sketch of J.J. Thomson's early experiments on pulsed plasmas in long vacuum tubes [1].

than 1.5×10^{10} cm/s, or in excess of half of the speed of light. Furthermore, Thomson determined that the luminous front always appeared to travel from the positively pulsed electrode (anode) to the ground electrode (cathode).

The study of these luminous fronts was revisited by several researchers in the wake of Thomson [27–29], but their attempts to duplicate the measured speeds were met with varied success. In 1930, Beams confirmed definitively confirmed those of Thomson. He also found that the front always initiated at the electrode with the highest, absolute potential, relative to ground. Beams hypothesized that the rapid motion of the front was a result of a self-propagating region of high space charge, quote:

> In the neighborhood of the electrode . . . the field is very high and intense ionization should take place. This ionization due to the large difference in mobilities of positive ions, negative ions and electrons respectively should result in the establishment of a space charge. This space charge, once formed near the high potential electrode . . . must move down the tube regardless of the polarity of the applied potential because of the changes it produces in the field near its edges.

At about the same time, Schonland and Collens reported on their observations of lightning [30]. Though the general structure and length scale of lightning is substantially differ-

ent from the luminous fronts observed by Beams and Thomson, the two phenomena would later prove to be very similar. In their work Schonland and Collens noted that lightning would usually occur in a two-step process. Based on the images they obtained, they suggested that the leader was generated by a relatively small "dart" with a mean vertical velocity of 7.2×10^8 cm/s. The dart moved in a random manner, changing directions at random intervals, but always moving toward the ground.

The second step began when this dart reached the ground. Once there, a bright return stroke would occur along the same path that the leader had traced out. In contrast to the leader stroke, the return stroke had a velocity of 5×10^9 cm/s. Schonland and Collens hesitantly attributed the leader stroke to an extended electron avalanche, and the return stroke to thermal ionization along the conductive path generated by the dart. However, calculations by Cravath and Loeb showed that the speeds of the proposed avalanche was inconsistent with the fields at the head of a lightning stroke [31]. Instead, they suggested that the dart was actually a moving region of space charge which locally accelerated electrons to ionizing energies. This was similar to the mechanism earlier proposed by Beams.

1.2.2 The Streamer Model

It was long known that sparks in air were similar to lightning. Advances in technology during the 1930's led to experiments which reinforced this similarity. In response to the measurements of Schonland and Collens; Snoddy, Beams, and Dietrich studied the breakdown of gas in a long tube with both positive and negative applied potentials [32]. Using an oscillograph, they observed both the leader and a return stroke in both cases. However, the propagation of the plasma wave toward the cathode required a source electrons ahead of the wave. The authors proposed that photoionization might provide these necessary electrons.

Around the same time, Flegler and Raether had come to a similar conclusion regarding the importance of photoionization. This led them to develop a more thorough theoretical model for these waves [33] which came to be known as the streamer theory. This was

followed by a similar treatment by Loeb and Meek [34–36]. The streamer theory divided the initial plasma formation into two steps. In the first step, an electron avalanche is initiated between two electrodes. The avalanche travels toward the anode and leaves behind a region of positive space charge. In the second step, the return stroke begins at the anode and travels along the conductive path generated by the initial avalanche toward the cathode.

The streamer model proved relatively successful in describing the development of sparks and lightning. Theoretical estimates of the speed matched the velocity measurements that were acquired with photographs and oscillographs. Additionally, the theory was able to account for the branching manner in which lightning was formed as well as the constriction in space.

Following the initial work of Flegler, Raether, Loeb, and Meek, a number of researchers began to explore the boundary between the Townsend mechanism and the streamer mechanism. Most notable was Fisher and Bederson's work in 1951 [37], which was later extended to nitrogen [38] and argon [39]. These studies suggested that the streamer theory was incomplete. Furthermore, the reliance of the streamer theory on photoionization would later prove very contentious [40]. Finally, there was a whole class of discharges that it did not readily explain.

1.2.3 Diffuse Streamers

As noted by Chalmers [41], Rogowski and Buss [42, 43] observed a fast, diffuse, glow discharge immediately prior to the filaments of a streamer discharge. Allibone and Meek, noted similar diffuse discharges in air based on oscillographs and photographs [44–46]. However, the Boys apparatus [47] which was employed in these studies (an ancestor to the modern streak camera) was unable to capture the evolution of the diffuse glow, given its large spatial extent.

This was first noted by Allibone who attempted to use Lichtenberg figures[2] to definitively

[2]Such figures directly exposed photographic emulsions to the electrical discharge. The developed image

capture this diffuse glow [48]. Later, Saxe and Meek used the recently invented photomultiplier tube to record the evolution of the light emissions in the brief, diffuse glow [49] as a function of space. Both studies agreed in the existence of the diffuse glow, despite some disagreement on the nature of its geometry and propagation.

By 1968 (according to Kunhardt and Byszewski [50]), Stankevich and Kalinin had provided the most firm evidence yet of a diffuse discharge in a dense gas [51]. This was later confirmed by experiments with a pulsed nanosecond discharge by Mesyats, Bychkov, and Kremnev [52]. In their analysis, they concluded that photoionization could not play a role in such short-lived discharges. The formation of their discharge only required several nanoseconds, much shorter than the lifetimes of the excited states responsible for photon emission. They suggested that the streamer model required some extension.

In addition to the diffuse discharge, Stankevich and Kalinin also noted the detection of x-rays with each pulse. This suggested the presence of high-energy electrons impinging on the surface of the electrodes, despite the high collisionality of the dense gas. Not only that, but the electron energies could even exceed what would be expected from the vacuum electric fields [53]. The eventual conclusion was that the electric field associated with the space charge at the head of the streamer produced very energetic electrons which deposited their energy far from the streamer tip [50, 54], allowing the streamer to spread out beyond the diffusive region of the electrons.

It was based on the studies of the fast electrons in these discharges that Mesyats, Bychov, and Kremnev proposed the use of a fast electron beam for pumping high-pressure gas lasers. Similar work was conducted simultaneously by Fenstermacher et al. [55]. Palmer [56], and Levatter and Lin [22] determined that there was a threshold amount of preionization required to ensure homogeneity of the discharge. Hunter [57], and Koval'chuk and Mesyats [58] later proposed that such discharges be used for fast-closing switches. Gas lasers and fast switches would drive much of the later research on fast, pulsed discharges.

---

was a time-integrated representation of the discharge.

Eventually these discharges came to be referred to as fast ionization waves (FIWS). A large body of Russian literature developed around their study, though much of it has remained untranslated. In 1994, Vasilyak produced an extensive review of these studies [16]. The data include wave velocities for a variety of gases and pressures. Other parameters such as attenuation coefficients for the waves, high energy electron currents, electric field measurements, and a circuit model of the FIW are also included.

1.2.4 RPNDS

Beginning in 1998, the Moscow Institute of Physics and Technology (MIPT) produced a flurry of studies on the FIW [18, 59, 60]. They employed several different diagnostic techniques (photomultiplier tubes and capacitive probes) in an exceptionally detailed study in both air and nitrogen, using a shock tube and a bell jar. A summary of these investigations can be found in [21]. The work showed exceptionally reproducibility of the discharge parameters at relatively low repetition rates, on the order of tens of Hz, and evidence of runaway electrons. This work also included some of the first approximations of the electron energy distribution function (EEDF).

Interestingly, later analysis of a anode-directed FIW in nitrogen by the group at MIPT [61] concluded that the, the vast majority of the electrons were generated *after* the wave. This suggests that the ionization in an FIW does not strictly track the luminous front of the wave. Additionally, measurements of the conductivity suggested that the local approximation becomes invalid in the wave front and the electron energy distribution function resembles a beam.

In 1997 the invention of the fast ionization dynistor (FID) was revealed [23]. These new devices enabled sub-nanosecond switching of 10's of kilovolts, with repetition rates approaching 100 kilohertz. This was a leap forward over previous technologies which generally used thyristors or spark gaps for switching. Particularly appealing was the high repetition rate of the FID.

Recall that the volume-filling FIW required a significant amount of preionization. This was often accomplished an ionization source in addition to the high voltage pulse (in the form of UV radiation, or electron beams). However, the repetition rates of FIDs were high enough such that a substantial number of electrons would carry over between pulses. These seed electrons obviated the need for a preionization. In addition, the time-averaged densities of excited states could maintained at much higher values. This had particular promise for processing applications.

In the eventual commercialization of the FID made economically feasible to create fast, repeatable fast ionization waves. It is this class of discharges which are now referred to as repetitively-pulsed nanosecond discharges, or RPNDS. Their uniformity, low gas heating, high-pressure operation, and efficient ionization made them attractive or a number of applications:

- plasma-assisted combustion [62],
- magneto-hydrodynamic energy bypass [63],
- plasma actuators [64],
- and high-pressure xenon lamps [65, 66].

As with the FIWs, the primary diagnostics were current and voltage characteristics, electric field measurements with capacitive probes, and emission measurements with photomultiplier tubes. Later, intensified CCDs were used to record the emissions of specific transitions as well as broadband light. This approach has been used to more clearly illustrate the uniformity and reproducibility of the discharge [64]. Other researchers have turned to laser-based diagnostics, such as coherent anti-Stokes Raman scattering, to measure gas heating [67] and the electric field in molecular systems [68, 69]. Likewise, laser collision-induced fluorescence (LCIF) has been used to obtain axial profiles of excited state and electron densities in helium RPNDS [70].

Concurrent with these improvements in experimental techniques has been similar progress in the simulation of RPNDS. The one-dimensional models

Fenstermacher et al. [55]. Later, Hunter [57], and Koval'chuk and Mesyats [58] proposed that such discharges be used for fast-closing switches. The need for a homogeneous plasmas in these applications prompted Palmer [56], and Levatter and Lin [22] to investigate the necessary conditions for uniformity. They concluded that the primary requirement for uniformity was a threshold value of fractional ionization.

1.2.5 Repetitively-Pulsed Nanosecond Discharges

The type of discharge originally studied by Babich, Loika, and Tarasova came to be known as the fast ionization wave (FIW). In the years following its discovery, a substantial effort was made to document the properties of the FIW over a wide range of conditions. In these studies, the wave velocity, current, and attenuation were the most frequently measured quantities. Much of this work is summarized in a review by Vasilyak [16]. Also reviewed are Slavin and Sopin's work which was the first to attempt a computation of the electron energy distribution function EEDF in FIWS [71].

The experimental measurements and computational work reported by Vasilyak were expanded on by a series of studies conducted at the Moscow Institute of Physics. These are reviewed by Starikovskaia et al. [21] and included measurements of the electron density, electric field, and energy coupling for FIWS in air, nitrogen, and hydrogen. The computational work by Starikoskaia and Starikovskii [72] still represents the most detailed study of the EEDF in nitrogen FIWS.

However, Starikovskaia et al. noted that the usefulness of FIWS were limited, in part, by their repetition rates. The power supplies for FIWS were capacitor banks, charged in parallel, and discharged in series (also referred to Marx banks). Unfortunately, the spark gaps used to trigger these capacitor banks would not operate above a few hundred Hz. This changed in the late 1990's with the development and commercialization of fast, solid-state switches.

Specifically, with the fast ionization dynistor it was possible to achieve repetition rates of 100 kHz [23].

This led to a new class of repetitively-pulsed discharges, or the RPND. These discharges operated at sufficiently high rates such that the electrons and ions would persist in significant quantities between pulses. This meant that the plasma duty cycle was increased by a significant amount. These improved qualities of the RPND over the FIW inspired a number of novel, application-driven studies. This included:

- Plasma-assisted combustion [15, 62, 73]
- Magnetohydrodynamic energy bypass engines [15, 63, 74]
- Plasma actuators [64, 75]
- High-pressure xenon lamps [65]
- Plasma medicine [10, 76]
- Water treatment [77]

Though not specific to the RPND, Becker et al. [7] provide an extensive discussion of the potential uses for non-equilibrium air plasmas.

As a result, contemporary researchers have produced a wealth of literature on the operation of RPNDS. More recently, there have been detailed measurements of the gas temperatures [67, 73, 78–83], chemical composition [80–82], electric fields [68, 84, 85], and energy coupling [73, 86]. Notably, these studies have been generally restricted to molecular gases; air, nitrogen, and occasionally, hydrogen.

The first such study was the work of Laroussi and Lu who examined a RPND excited in a stream of helium flowing from a tube into air [87, 88]. The resulting plasma had the appearance of a jet, emitted from the open end of the tube. Using fast photography they observed that the jet was actually a series of plasma "bullets" formed with each pulse. Measurements of the bullet velocities showed that their speed greatly exceed what would be

expected purely from electrons drifting under the applied electric field. They described the bullet as a classic cathode-directed streamer propagated by photoionization.

The plasma bullets of Laroussi and Lu spawned a great deal of interest in RPND helium plasma jets[3] For example, Walsh et al. studied the atomic oxygen production for helium-oxygen mixtures with the use of emission spectroscopy and a global plasma chemistry model [89]. Urabe et al. employed a variety of laser diagnostics to measure the radial density profiles of helium metastable atoms and molecular nitrogen ions in a similar jet. This work was supported by a number of two-dimensional plasma simulations such as those by Naidis [90] and Breden, Miki, and Raja [91].

Simultaneously, there has been a decline in the study of FIWs, and relatively little on large-volume RPNDs. One of the most recent FIW studies was produced by Takashima et al. [92]. In it, the authors reported on FIWs in helium and nitrogen which were studied using capacitive probes and voltage-current characteristics. The results were compared to extensive two-dimensional fluid simulations and an analytic, one-dimensional drift model. In most cases, the measurements and simulations showed good agreement.

1.3 Summary

Contemporary RPND studies have mostly focused on measurements in the afterglow plasma or of time-integrated quantities. This has limited the understanding of how RPNDs develop as only so much can be inferred from these measurements. Particular issues, such as the electron energetics in the wave front are not firmly known. Relatedly, the relative importance of photoionization and nonlocal electrons is still under debate. Even measurements of common plasma parameters such as electron densities and temperatures are in short supply. Each of these issues is important in the development of a thorough theoretical understanding

[3] A distinction should be made between plasma jets, excited by sinusoidal power supplies, similar to the well-known dielectric-barrier discharge [13], and those produced by nanosecond pulses. Differences between the two were reported by Walsh, Shi, and Kong [17].

of RPNDs, as well as the validation of simulations, and optimization for real world applications.

Relatedly, the study of RPNDs has generally been limited to molecular gases such as air, nitrogen, oxygen, or combustion-related mixtures. Consequently, little information has been published on rare gas RPNDs, in spite of the fact that their unique physics makes them ideal for certain uses. For example, rare gas discharges exhibit very little gas heating, making them desirable for the treatment of highly sensitive materials. Additionally, the radiative emissions of rare gases have a range of uses from commercial lighting to gas lasers. Finally, the large degree of Penning ionization resulting from rare gases may make them useful in RPND gas mixtures as a means of optimizing discharge properties.

In order to address these issues, this work will use a combination of experiments and modeling to examine the plasma dynamics of a helium RPND on time scales ranging from 5 ns to 100 μs and at pressures from 0.3 to 16.0 Torr. The nanosecond time scale results will be one of a very few datasets available on the evolution of the RPND during its formation. This will provide new insight on the dominant physical processes in the wave front. To complement this, the microsecond time scale measurements will reveal the dominant loss mechanisms in between pulses as well as the time-averaged characteristics of the RPND. Lastly, the parameterization with pressure will offer the chance to examine how the physics of the discharge is altered by the collisionality.

Experimentally, the RPND will be studied by its current and voltage characteristics, optical emissions, and with laser absorption spectroscopy. The current and voltage characteristics will be used to determine the energy absorbed by the plasma with each pulse. The optical emissions will provide information about the excited state dynamics and the wave velocity. Finally, the laser absorption spectroscopy will be used to resolve the short time scale dynamics and as a benchmark for the numerical modeling. The modeling will focus on the development of a detailed global model of a helium discharge. This model will be informed by additional particle-in-cell simulations, and solutions of the Boltzmann equa-

tion. Using the metastable measurements as a baseline, the global model will be used to predict the electric field, electron temperature, electron density, excited state densities, and emissions of the RPND.

CHAPTER 2

Theory

In order to properly understand the RPND–the experimental measurements, and the models, it is necessary to develop a theoretical underpinning. The RPND is an ionized gas, and, dependent on its characteristics, a plasma. Therefore, we begin with a review of the statistical description of an ionized gas, equilibrium solutions, and several approximations. Subsequently, the discharge initiation process is considered from the perspective of a single avalanche. The Townsend model is briefly reviewed, followed by a more detailed explanation of the streamer model. This naturally leads to the development of a homogeneous discharge condition based on the preionization density–the basis for the RPND. Following this, a qualitative introduction to atomic structure is provided in order to introduce spectroscopic concepts such as energy levels, transitions, lineshapes, and absorption cross sections.

2.1 Ionized Gas

An ionized gas is a volume of gas in which some fraction of the neutral atoms and/or molecules have been separated into electron and ion pairs. For a sufficiently large number of particles and collision rate, the behavior of each species in the ionized gas can be described by a continuous distribution function.

This function is an expression of the likelihood of finding a particle within a specific range of velocities in a specific volume, as a function of time. This function is denoted as

$f_\alpha(\vec{r},\vec{v},t)$, where the subscript α denotes the species, f is the distribution function, $\vec{r}$ is the position, $\vec{v}$ is the velocity, and t is the time.

The behavior of f_α can be shown [93] to be governed by the Boltzmann equation,

$$\frac{\partial f_\alpha}{\partial t} + \vec{v}\cdot\nabla f_\alpha + \frac{q_\alpha}{m_\alpha}\left(\vec{E}+\vec{v}\times\vec{B}\right)\cdot\nabla_v f_\alpha = \left(\frac{\partial f_\alpha}{\partial t}\right)_{\text{coll}}. \tag{2.1}$$

Here, m is the particle mass, q is its charg:, $\vec{E}$ is the electric field, $\vec{B}$ is the magnetic field, and $(\partial f_\alpha/\partial t)_{\text{coll}}$ is a term which represents changes to the distribution function as a result of collisions. Coupled with Maxwell's equations, equation 2.1 provides a complete description of the behavior of the fields and particles in a plasma.

For a species in equilibrium in the absence of external forces and $(\partial f_\alpha/\partial t)_{\text{coll}} = 0$, it can be shown [94] that the distribution of energies is

$$f\alpha(\varepsilon) = C\varepsilon^{1/2}\exp\left(-\frac{\varepsilon}{k_{\text{B}}T_\alpha}\right) \tag{2.2}$$

where C is a normalizing constant, ε is the energy, k_{B} is Boltzmann's constant, and T_α is the temperature of the species. This is referred to as the Maxwell-Boltzmann distribution. It should be emphasized that this solution only applies when the classical species can be considered to be in equilibrium. Gradients and electromagnetic fields can both significantly alter the distribution function of a species. This can be of particular importance in the calculation or reaction rates, or the measurement of temperatures.

Additionally, the Boltzmann equation may be solved for electrons in equilibrium constant electric field, provided that a constant current density, and only elastic collisions. This is generally valid if the electric field strength is sufficiently small such that the mean energy of the electrons does not become comparable to the threshold energies for inelastic collisions. This result was originally presented by Druyvesteyn and Penning [94] and has come

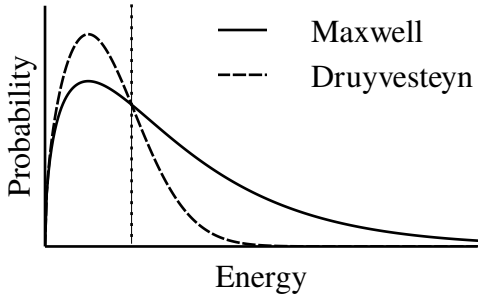

Figure 2.1: Comparison of the Maxwell-Boltzmann energy distribution and the Druyvesteyn distribution for the same average energy (illustrated by the dotted line).

to be known as the Druyvesteyn distribution. It is defined as,

$$f_\alpha(\varepsilon) = C\varepsilon^{1/2} \exp\left(-\frac{\varepsilon^2}{\langle\varepsilon\rangle^2}\right) \tag{2.3}$$

where $\langle\varepsilon\rangle$ is some mean energy, determined by the gas properties. This solution tends to suppress the probability of higher and lower-energy electrons in favor of more intermediate values. Figure 2.1 compares the probability distributions from equations 2.2 a]nd 2.3 for the same temperature T_α. The dotted line illustrates the average energy for the two distributions, which is not the same as the most probably energy.

Additional solutions of equation 2.1 in anything but these simple cases can be very challenging (c.f. chapter 18 of [95]). Even computational approaches can be stymied by the seven-dimension phase space and high dynamic range. In most situations, the Boltzmann equation is reduced to more tenable expressions by integrating over velocity-space (leaving f as a function of space and time). The first so-called moment is the conservation equation or continuity equation [**?**],

$$\frac{\partial n_\alpha}{\partial t} + \nabla \cdot (n_\alpha \vec{u_\alpha}) = G_\alpha - L_\alpha. \tag{2.4}$$

In this case, there is now a mean velocity $\vec{u}$, as well as gain (G) and loss (L) terms which

replace the collision operator. The gain and loss terms are generally expressed as the product of the densities of the interacting species, and a rate coefficient. For an electron-impact interaction where the target is relatively stationary, the rate coefficient is

$$K = \int_0^\infty f_e(\varepsilon)\sigma(\varepsilon)\sqrt{\frac{2\varepsilon}{m_e}}d\varepsilon, \tag{2.5}$$

where σ is the energy-dependent cross section.

The definition of the mean velocity, $\vec{u}$ can be obtained by multiplying equation 2.1 by v and integrating over velocity-space, to obtain the second moment [95],

$$m_\alpha n_\alpha \left[\frac{\partial \vec{u_\alpha}}{\partial t} + (\vec{u_\alpha}\cdot\nabla)\vec{u_\alpha}\right] = q_\alpha n_\alpha(\vec{E} + \vec{u_\alpha}\times\vec{B}) - \nabla\cdot\vec{\Pi} + \vec{f}|_{\text{coll}}. \tag{2.6}$$

This expresses the conservation of momentum by the plasma. It provides a means by which to solve for the mean velocity of the system, however it also introduces two additional terms. $\vec{f}|_{\text{coll}}$ deals with the forces transferred to α via collisions. This is often approximated as the Krook collision operator, which is only dependent on known quantities: m, n, $\vec{u}$, G, L, and the momentum transfer frequency, ν_{m}, for the species α and all species it interacts with. The second term, $\vec{\Pi}$, is the pressure tensor and can only be defined by the third moment of the Boltzmann equation. In fact, each additional moment introduces a new term requiring a higher order moment, *ad infinitum*. In most situations, this chain of equations is terminated after the first two or three moments by the use of an additional assumption such as an equation of state. One common example of an equation of state is the isothermal relation, $p = nk_{\text{B}}T$, which can be used to remove the pressure tensor.

For the purposes of this paper, one more moment will suffice. Assuming that the pressure is isotropic, one can multiply equation 2.1 by $mv^2/2$, and integrate over velocity-space to find the energy conservation equation,

$$\frac{\partial}{\partial t}\left(\frac{3}{2}p_\alpha\right) + \nabla\cdot\frac{3}{2}(p_\alpha\vec{u}_\alpha) + p_\alpha\nabla\cdot\vec{u}_\alpha + \nabla\cdot\vec{q}_\alpha = \frac{\partial}{\partial t}\left(\frac{3}{2}p_\alpha\right)\Big|_{\text{coll}}. \tag{2.7}$$

In this case, p represents the isotropic pressure, and $\vec{q}$ is the heat flow. The first term on the LHS represents the total energy contained by the species, the second term is the energy flux in and out of the volume, and the third term accounts for changes due to compression or expansion. The RHS is the collision operator which describes energy added or removed from the system as a result of collisions.

Equations 2.4 and 2.7 are particularly important for this study. As will be detailed in chapter 6, the two can be used to create a global model of the plasma. Such a model assumes spatial homogeneity of the plasma in order to reduce the associated computational costs. This allows the model to address large numbers of species over long periods of time as will be required in the case of the RPND.

2.2 Plasma Criteria

Though the Boltzmann equation describes both an ionized gas and a plasma, the two are distinct as a plasma is necessarily an ionized gas, but not vice versa. A plasma is unique in that its dynamics are governed by long range electromagnetic forces, unlike gases in which short-range collisions dominate. As a result, plasmas frequently exhibit large scale structure and organization. Examples of these structures are ubiquitous in astronomy where phenomena such as the aurora borealis, coronal mass ejections, and even interstellar media are all plasmas [96]. There are three criteria which form a more exact definition of what constitutes a plasma.

2.2.1 Debye Length

If an electrical perturbation is introduced into an ionized gas, the charged particles will tend to rearrange themselves to shield it out. A plasma is an ionized gas which is large enough for this shielding effect to occur. The characteristic length scale for this shielding effect to take place is referred to as the Debye length, denoted λ_D. It can be shown to be equal to

$\sqrt{\varepsilon_0 T_e/(en_0)}$, where ε_0 is the vacuum permittivity, T_e is the electron temperature, and n_0 is the plasma density. If the characteristic length scale of the ionized gas is L, then $\lambda_D < L$ for it to be considered a plasma.

2.2.2 Debye Sphere

However, the above condition by itself is not sufficient for shielding to occur. It is possible that an ionized gas may have a relatively small Debye length, but also lack enough charged particles for shielding to occur. More simply put, it would be impossible for a single electron to shield out even the smallest of perturbations. For that reason, the number of particles in a Debye sphere must be greater than unity in a plasma, or $n_0(4\pi\lambda_D^3/3) >> 1$.[1]

2.2.3 Plasma Oscillations

Finally, a plasma may exhibit Debye shielding, but lack the collective behavior of a plasma. This can occur when the collision frequency with neutral particles is too high. In this case, the behavior of the ionized gas would be determined more by the random collisions. Therefore, the characteristic response frequency of a plasma, commonly called the plasma frequency, must be greater than the neutral collision frequency, or $\omega_p > \nu$. The plasma frequency can be shown to be $\omega_p = \sqrt{e^2 n_0/(\varepsilon_0 m_e)}$.

There are many natural and man-made plasmas of varying size and quality. Figure 2.2 shows several categories of plasma, plotted as a function of their electron density and temperature. As can be seen in this example, the electron densities span seven decades, and the densities cover in excess of 20. This broad range of conditions presents a particularly challenging problem for both simulations and experimental measurements. Also highlighted in the figure is the range spanned by the RPND.

[1] This condition is also implied in the derivation of the Debye length.

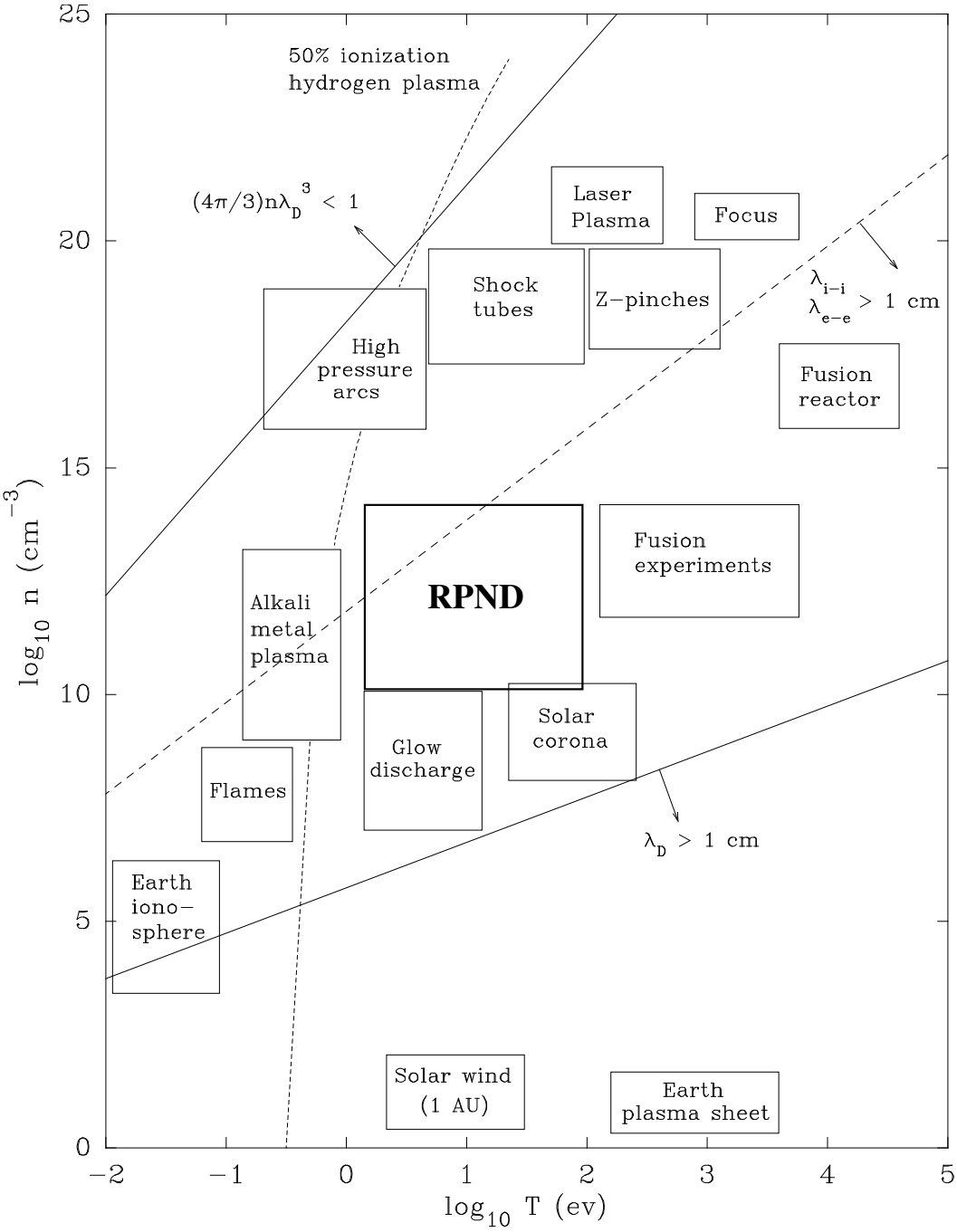

Figure 2.2: Illustration of the various regimes of plasma in terms of electron temperature and density with the RPND regime highlighted [2].

2.3 Discharge Initiation

The Boltzmann equation is a continuous, statistical description of a plasma. By comparison, the initial breakdown of a plasma is a highly discontinuous process marked by its stochasticity. The initiation of a discharge is typically the result of electron avalanches which occur randomly throughout a volume of gas. Often, the seed electrons for a plasma are the products of ionizing cosmic rays. At sea level this results in a few electrons per cubic-centimeter. As a result, it is necessary to consider the initiation of a discharge separately from a pre-existing plasma.

2.3.1 Townsend Mechanism

Classically, plasmas are created by two different mechanisms, the applicability of which depends on primarily on the strength of the electric field relative to the neutral gas density, a value called the reduced electric field. At lower reduced fields, the Townsend mechanism is responsible for the formation of a plasma. Consider two electrodes separated by a gap filled with some gas. An electron starting near the cathode will drift toward the anode. For a large enough electric field the electron will gain sufficient kinetic energy to ionize a neutral atom, producing a second electron. The two electrons are now accelerated by the field, instigating further ionization of the background gas. The population of electrons quickly grows, thus the process is referred to as an electron avalanche. Eventually, the avalanche electrons are collected at the anode.

In their wake are ions which slowly drift toward the cathode. As the ions impact the surface of the cathode, they occasionally cause a secondary electron to be emitted. This secondary electron initiates a new avalanche and helps to sustain the discharge. A steady state electric discharge occurs when the electron multiplication in the avalanche compensates for the finite probability that an ion striking the cathode releases a secondary electron. Therefore, the characteristic time for a Townsend discharge to develop is approximately

equal to the time it takes an ion to drift across the gap (for a gap of several cm this can be on the order of 10^{-4} s).

The Townsend mechanism is characterized by two parameters: α and γ, the first and second Townsend coefficients. α is the number of ionization events that occur per unit length, often expressed as a function of the reduced field. The second Townsend coefficient is the probability that an ion impinging on the cathode produces a secondary electron. The values for γ can vary widely and depend on the type of ion, its energy, the cathode material, contamination of the surface, and many other factors. That said, typical values are around 0.01-0.1.

2.3.2 Streamer Mechanism

In contrast, the streamer discharge which occurs for larger values of the reduced field does not depend on secondary emission. Additionally, streamer discharges can develop in time periods as short as 1 ns, much less than the time required for Townsend breakdown. In order to describe the streamer mechanism, again consider an electron between two electrodes, as seen in (a) of figure 2.3. As with the Townsend discharge, this electron initiates an avalanche which moves toward the anode. As the electrons travel toward the anode, they randomly collide and diffuse, leaving behind a cone of ions, as seen in part (b). However, the higher reduced field drastically increases α. This causes the space charge of the avalanche to create an electric field comparable to the one that is applied, quickly halting the avalanche.

Once stalled, the avalanche can no longer continue to advance toward either electrode. At this point the avalanche can be considered a streamer as it begins to increase its extent by several other processes. The large internal fields of the avalanche can accelerate individual electrons and "inject" them in the direction of the anode [50]. In addition, as the excited atoms in the wake of the avalanche begin to radiate, they can cause photoionization throughout the volume. Photoelectrons generated close enough to the negative head, or positive tail of the streamer will initiate secondary avalanches which eventually connect to the primary

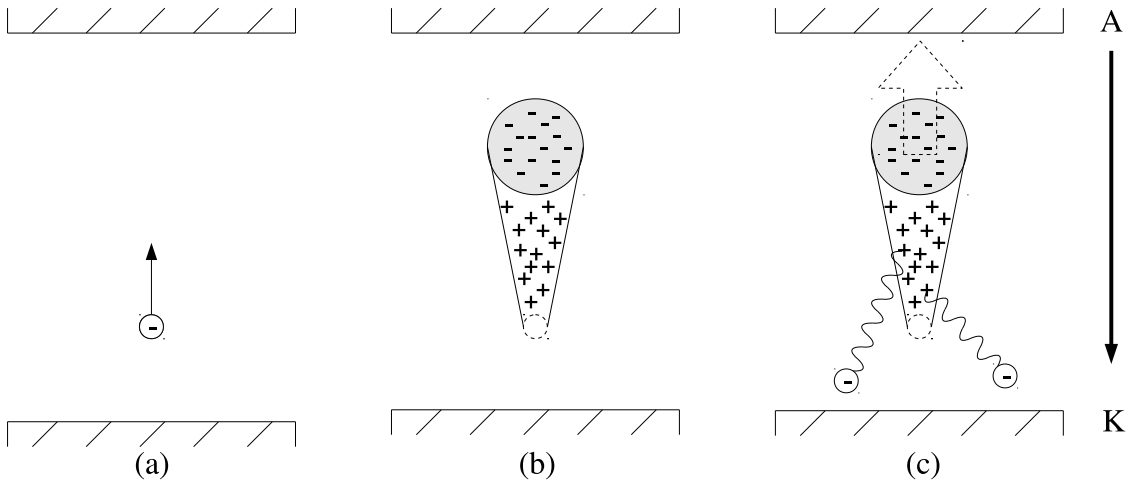

Figure 2.3: An illustration of the development of a single streamer. (a) A seed electron is accelerated by the applied electric field. (b) The initial electron develops into an avalanche which leaves a large region of positive space charge, halting further advance. (c) The streamer propagates toward the cathode via photoionization and the anode via nonlocal electrons and photoionization.

one. Both of these methods take place primarily along the axis of the original avalanche, thus the streamer remains relatively constricted in the direction transverse to the electric field.

2.3.3 Homogeneity Condition

However, these processes are not critical in the formation of a large-volume discharge by an RPND. This description of a streamer only considers an avalanche generated by a single electron. In reality, many can form simultaneously assuming that there is more than one seed electron in the volume. With sufficient preionization of the volume, the strong fields of the individual avalanches can begin to overlap. This smoothes out the field gradients which would otherwise radially constrict the streamers. Instead, ionization progresses homogeneously throughout the volume.

In order to determine the necessary preionization density, we refer to the work done by Levatter and Lin on gas laser discharges [22]. First, the electron drift velocity in an applied field can be expressed as the product of the field and the electron mobility μ. The electron

mobility is the steady-state drift velocity for an electron in an applied field and represents the balance between the frictional force of the neutral gas collisions and the electric field. Consequently, the mean velocity of electrons drifting in a time-varying field $E(t)$ can be expressed as

$$u(t) = \mu(E)E(t). \tag{2.8}$$

This allows the length of the avalanche can then be written as an integral quantity,

$$\xi = \int_{t_0}^{t} u(t)dt. \tag{2.9}$$

Here, t_0 is the time at which $E(t)$ becomes high enough that the first Townsend coefficient, α, exceeds 0. Because no electron multiplication occurs while $\alpha < 0$, this effectively represents the beginning of the avalanche.

The electric field in the head of the avalanche depends on its radius, which is dependent on the diffusion of the electrons as they cross the gap. This is governed by the free diffusion coefficient, $D = \lambda v_m athrmth(E)/3$, where λ is the mean free path of the electrons, and v_{th} is their thermal velocity. The diffusion radius is then equal to

$$R(\xi) = \int_{0}^{\xi} \lambda v_{\mathrm{th}}(\xi')d\xi'. \tag{2.10}$$

For the calculations below, λ is assumed to be fixed. In contrast, the thermal velocity of the electrons is expected to grow as the electric field deposits energy in the electrons. As a result, it is necessary to integrate the diffusion coefficient over the avalanche in order to determine R.

Levatter and Lin assume that the avalanche stalls when the peak field of the avalanche is equal to the applied field. Assuming that the electrons diffuse equally in all directions,

the electric field of the avalanche head can be expressed as

$$E_a(r) = \frac{eN_e}{4\pi\varepsilon_0 R^2} F(r/R), \qquad \text{where} \tag{2.11}$$

$$F(r/R) = \frac{1}{R^2}\left[\mathrm{erf}(r/R) - \frac{2}{\pi^{1/2}}(r/R)\exp(-r^2/R^2)\right], \tag{2.12}$$

where r is the radius with respect to the center of the avalanche, N_e is the number of electrons in the avalanche, erf is the error function. F is a dimenionless function which has a peak value of 0.428. Provided α as a function of reduced field, the number of electrons in the avalanche is equal to

$$N_e = \int_0^{\xi} \alpha(\xi')d\xi'. \tag{2.13}$$

Here, Levatter and Lin make a number of assumptions in order to develop an analytic and dimensionless solution for $E_{a,\max}(t) = E(t)$. However, it is possible to numerically integrate equations 2.9, 2.10, and 2.13 to determine the time required for the avalanche to stall. This should provide a more accurate, but less general result. Assuming a linearly increasing electric field, figure 2.4 shows the results of such calculations for an avalanche in 1.0 Torr of helium, as a function of various breakdown delays. The breakdown delay is defined as the time it takes for $\alpha > 0$. The mobilities, mean velocities, and Townsend coefficients were interpolated from solutions of the Boltzmann equation provided by the BOLSIG+ code with Phelps' cross sections [97]. For this range of breakdown delays, the avalanche was able to develop up to 6 cm in length before it stalled. The times required for the avalanche to stall ranged from around 13 ns for the shortest breakdown delay, and 330 ns for the longest.

From this, a criteria for homogeneous breakdown of the gas can be developed. In order for the field gradients to be smoothed out, the individual avalanche heads should roughly overlap by the time they have stalled. Assuming that all seed electrons in the volume initiate avalanches, this is equivalent to the requirement that $n_{e,c} > r_c^{-3}$, where $n_{e,c}$ is the critical electron density, and r_c is the avalanche radius at stall. As seen in figure 2.4, this suggests that a preionization density of 10^{11} to 10^{15} is required for the breakdown times under con-

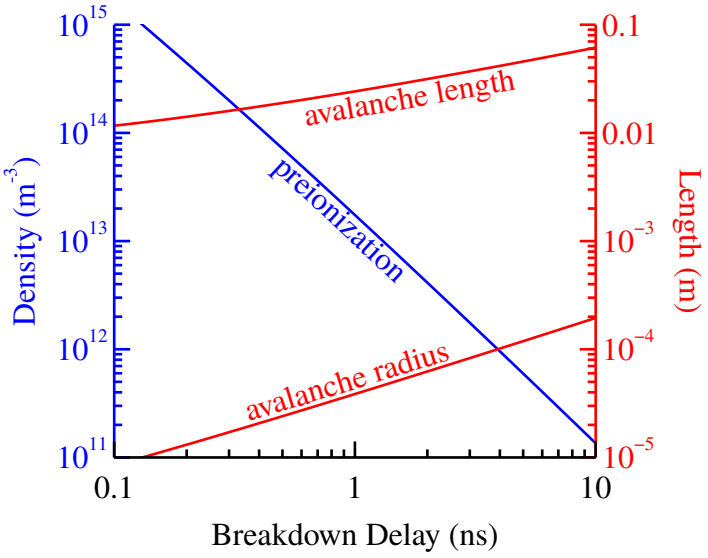

Figure 2.4: Numerical calculations of the preionization density for homogeneous excitation, avalanche length, and avalanche radius in helium at a pressure of 1.0 Torr as a function of the slope of the electric field.

sideration.

Based on this formulation for the homogeneous breakdown condition, tt is apparent that as the avalanche radius increases, the necessary preionization density decreases. It is less obvious as to why the avalanche radius decreases as the breakdown delay increases. This can be explained by the lower slope, implied by the long breakdown delays. As the slope decreases, the avalanche has a longer period of time to diffuse in the system, thus the increased radius.

2.4 Atomic Spectroscopy & Notation

As described, much of the experimental work presented will concern the use of spectroscopic techniques. Careful measurements of the light emitted from excited atomic states can yield electron densities and temperatures, excited state densities and temperatures, electric fields, and magnetic fields. The topic of spectroscopy is extensive and it is neither necessary nor desirable to cover it in full. Instead we will only consider what is necessary to

understand the emissions from a singly-excited, multi-electron atom.

An atom is composed of a small, positively charged nucleus, orbited by negatively charged electrons. The actual position of any single electron is probabilistic and described by a wavefunction or state; solutions of the Schrödinger equation for the atom in question. Many different wavefunctions exist, each described by four quantum numbers:

- $n = 1, 2, \ldots$: the principal quantum number,
- $l = 0, 1, \ldots, n-1$: the azimuthal angular momentum,
- $m_l = -l, \ldots, l$: the magnetic quantum number, and
- $s = \pm 1/2$: the spin quantum number.

The quantum numbers are hierarchical such that each n, or shell, possesses a series of subshells, l, while each subshell possesses a number of individual orbital, m_l, and each orbital possess one of two spins. As a result of the Pauli exclusion principle, the wavefunction of each electron around an atom is described by a *unique* set of quantum numbers. This means, that any particular subshell can only contain $2(2l+1)$ electrons. The subshells are often referred to using the nomenclature $0, 1, 2, 3, \ldots = s, p, d, f, \ldots$.

As a result of their separation from the nucleus, the electrons in an atom have some degree of potential energy. As the n and l of an electron increase, so does its potential energy. In most cases, m_l and s do not affect the potential energy of an electron. As an example, an electron in the 1s ($n = 1$ and $l = 0$) subshell has the lowest possible potential energy.

Absent from external influences, the individual states are populated with electrons so as to minimize the total potential energy of the system. This natural arrangement is referred to as the ground state configuration. Often, but not always, the subshells are filled sequentially and in order from lowest to highest l. Provided some input energy in the form of a collision or a photon, one or more of the electrons surrounding the atom may transition to another

state, increasing the potential energy of the system. In low-temperature plasmas it usually one of the electrons from the outermost or unfilled subshell to be excited.

In hydrogen and alkali metals, several subshells are filled with the exception of a lone outer (or valence) subshell with a single electron. For these atoms, the potential energy of any singly-excited configuration is uniquely determined by this electron. As a result, the initial and final states of the atom can be uniquely identified based on the initial and final n and l of the aforementioned electron. In contrast, the potential energies of configurations in other atoms are determined by the collective effects of all outer electrons. This includes the total azimuthal angular momentum $L = \sum l_i$, the total spin, $S = \sum s_i$, and the total angular momentum, $J = L + S$, where i are all the electrons of the valence shell. In addition, each state can be said to have either even or odd parity, defined as $(-1)^{\sum l_i}$, where -1 is odd, and 1 is even.

Together, these values are sufficient to identify the potential energy of the electron configuration. They are written with the internal shell configuration, followed by the "term symbol" for the outer subshell. One example of this term symbol is $1s2s^3S_1^o$, which describes the triplet helium metastable state. In this case, there is a single electron in the 1s subshell and a second atom in the 2s subshell. The configuration has a total azimuthal angular moment of 0 (denoted by the 'S'), an odd parity (denoted by the superscript 'o'), a total spin of $1/2$ (the superscript 3 is equal to $2S + 1$) and a total angular moment of 1.

The total angular momentum can often take on a range of values, called levels, depending on the individual l and s states. This is caused by a process known as spin-orbit coupling. The energy difference between configurations with different total angular momenta is very small, generally less than 1 eV. In addition, within each level is a number of degenerate configurations; configurations with different arrangements of electrons, but the same energies.

Excited atomic states usually have finite lifetimes. If possible, electrons will undergo transitions to lower the potential energy of the system. This can occur spontaneously, through the emission of a photon, or through a superelastic collision with another parti-

cle. In the case of spontaneous transitions, only certain states can transition to others, as defined by a series of selection rules:

- $\Delta S = 0$
- $\Delta L = \pm 1$ or 0
- $\Delta J = \pm 1$ or 0
- $L = 0$ cannot transition to $L = 0$
- $j = 0$ cannot transition to $J = 0$

These rules are determined from a lower order approximation, and thus are not strict. As a result, forbidden transitions can occur, however these generally take place at much lower rates.

Figure 2.5 is a Grotrian diagram of the energy levels in neutral helium and the allowed transitions. In this case, the atomic states are separated into the singlet ($S = 0$) and triplet ($S = 1$) manifolds. The singlet manifold represents excited states where the electron spins are anti-parallel, and the triplet manifold represents excited states where the electron spins are parallel. As indicated by the first selection rule, transitions between these two manifolds is forbidden, thus each is something of a self-contained system.

Also observable in the diagram are two "metastable" states. These are the 2s states at the bottom of the singlet and triplet diagrams. An electron in either state cannot spontaneously transition to a lower energy state. As a result, an electron in either state can be extremely long-lived. In addition, they are also the lowest-lying excited states of helium. For these reasons, helium plasmas tend to have high densities of metastable atoms. This makes them a good candidate for spectroscopic study as will be seen in chapter 4.

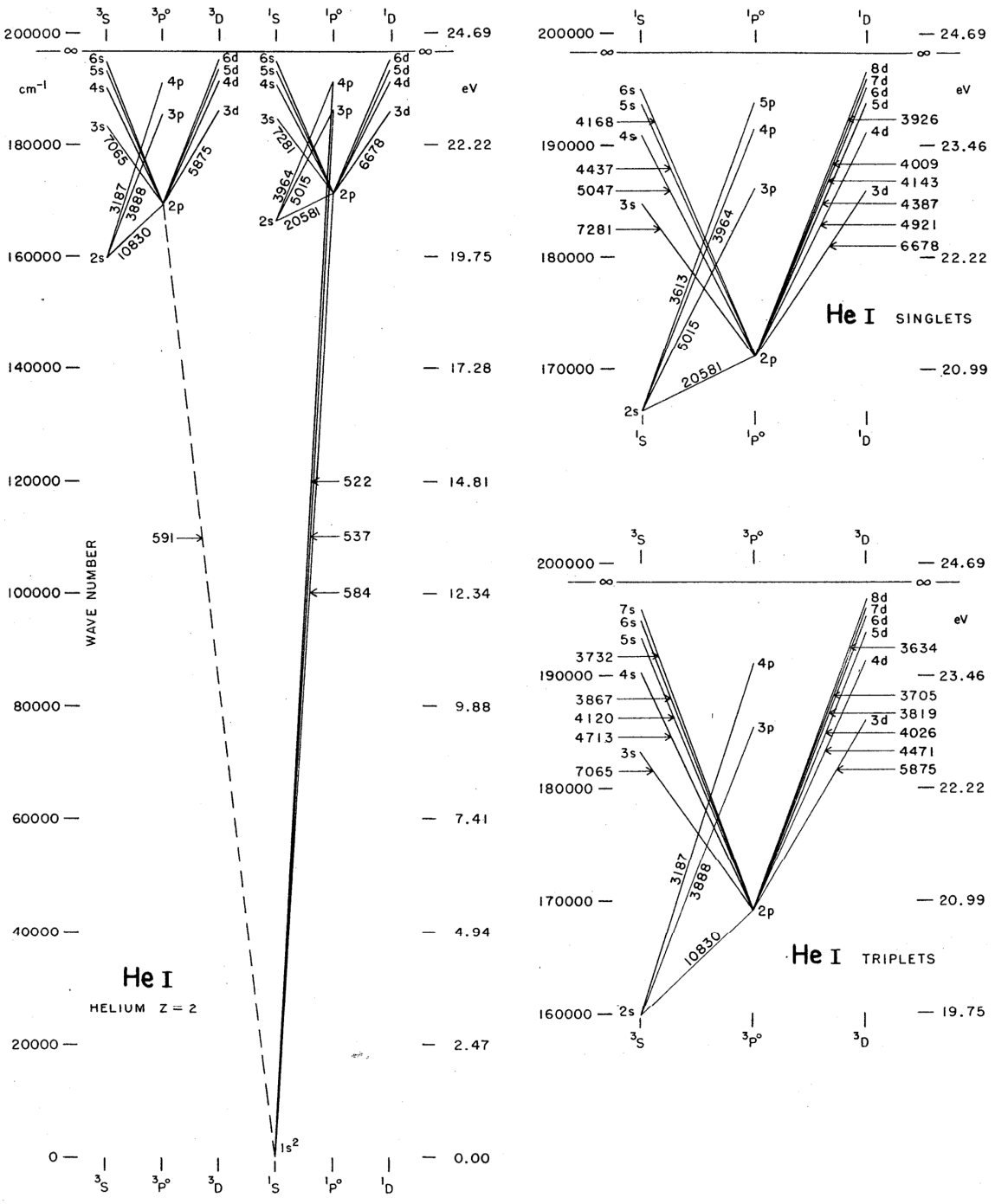

Figure 2.5: A partial Grotrian diagram of neutral helium [3].

2.4.1 Spectral Lineshapes

Electrons which transition to lower energy states emit photons which can be detected. Conversely, if an atom is exposed to a photon with an energy matching a transition, the atom may absorb the photon. Both processes are useful in determining the prevalence and dynamics of the excited states. This, in turn, can be used to infer various plasma properties.

Conservation of energy requires that the energy of the absorbed or emitted photon match the energy difference between the two states. However, the finite lifetime of excited atomic states implies, via the time-energy formulation of the uncertainty principle, some uncertainty in the actual energy difference between the states. As a result, the emitted photon will possess an energy selected from a distribution of energies.

This distribution is referred to as the spectral lineshape. The narrowest permissible lineshape, or natural lineshape, of an atomic transition can be shown [98] to be a Lorentzian of the form,

$$g(\omega) = -\frac{1}{4\pi^2}\frac{A\lambda^3}{\Delta\omega_a}\frac{1}{1+\left[2(\omega-\omega_a)/\Delta\omega_a\right]^2}, \tag{2.14}$$

where ω is the photon frequency, A is the Einstein coefficient for the transition, λ is the wavelength of the transition, ω_a is central frequency of the transition, and $\Delta\omega_a$ the full-width half maximum (FWHM) of the transition. In the ideal case, where the atoms motionless and unaffected by external perturbations, $\Delta\omega_a = A$. This is known as the natural linewidth.

Other processes can act to broaden or alter the spectral lineshape. For example, inter-atomic collisions can reduce the lifetimes of excited states. This results in additional broadening of the line, though it retains its Loretnzian nature. As the frequency of inter-atomic collisions increases linearly with pressure, this phenomena is referred to as pressure broadening. It can be included in equation 2.14 by using $\Delta\omega_a = A + BP$, where B is a measured or calculated broadening coefficient, and P is the pressure.

Atomic motion can also play a role in the spectral lineshape. If an atom is moving toward or away an observer as it emits a photon, the emitted photon will be blue or red

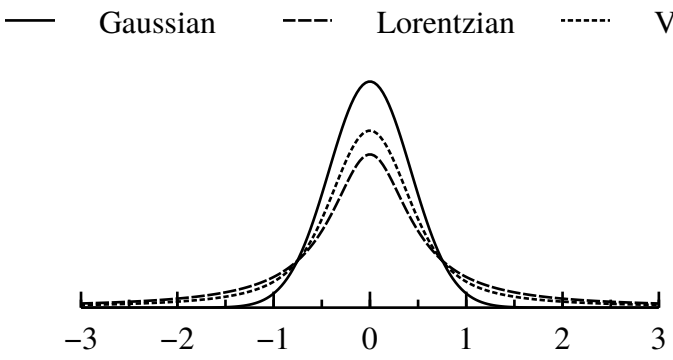

Figure 2.6: A comparison of the three primary spectral lineshapes, each with the same full width.

shifted. Likewise, if the atom is moving toward or away an incident photon, the energy of that photon will be shifted. If this effect is averaged over the random motion of atoms in a gas, the result is an additional broadening of the lineshape, called Doppler broadening. Unlike pressure broadening, Doppler broadening introduces a Gaussian component to the lineshape such that,

$$g(\omega) = \sqrt{\frac{2\ln 2}{\pi^3}}\frac{\Delta\omega_a}{\Delta\omega_d}\int_{-\infty}^{\infty}\frac{1}{[(\omega-\omega_a)-\omega']^2+4\Delta\omega_a^2} \times \exp\left[4\ln 2\left(\frac{\omega'}{\Delta\omega_d}\right)^2\right]d\omega'. \quad (2.15)$$

Here, $\Delta\omega_d = \omega_a\sqrt{\frac{8k_B T_g \ln 2}{Mc^2}}$, is the width of the Doppler broadening. This form of the spectral lineshape is known as the Voigt profile, and it must be numerically integrated. In the case that $\Delta\omega_d >> \Delta\omega_a$, equation 2.15 can be simplified to a standard Gaussian distribution,

$$g(\omega) = \sqrt{\frac{4\log 2}{\pi\Delta\omega_d^2}}\exp\left[-(4\log 2)\left(\frac{\omega-\omega_a}{\Delta\omega_d}\right)^2\right]. \quad (2.16)$$

The effect of the various broadening mechanisms is most apparent in the wings of the lineshape, far from the peak. Figure 2.6 illustrates the three major lineshapes with equivalent full widths. The Voigt profile is composed of equally broad Lorentzian and Gaussian

distributions. As can be seen, the wings of the Gaussian distribution fall off very quickly. In comparison, the Lorentzian component is observable well out to the edges of the figure.

The spectral lineshape can be altered by a number of other processes. Electric fields can influence the emissions via the Stark effect, while magnetic fields can split up degenerate states via the Zeeman effect. The fields of electrons and nearby molecules can also alter the lineshape of a transition. While not used in this study, such effects can be used as effective diagnostic tools for plasmas.

2.4.2 Absorption

As has been mentioned, a photon which closely matches the energy between two states can be absorbed by an atom. This property forms the basis for absorption spectroscopy where light with a known spectrum is used to illuminate a sample. The spectrum of the light that passes through the sample is measured and used to infer properties of the sample. In contrast to the emission processes occur spontaneously with a characteristic lifetime, often 10s of nanoseconds or more, absorption is almost instantaneous. This makes absorption-based spectroscopic methods desirable for fast phenomena, such as the RPND.

The cross section for a single atom to interact with a photon can be shown [98] to be,

$$\sigma(\omega) = A\frac{\lambda^2}{8\pi}\frac{g_1}{g_2}g(\omega). \tag{2.17}$$

where g_1 and g_2 are the number of degenerate configuration for the lower state and upper state respectively. $g(\omega)$ is the appropriate spectral lineshape, determined from the operating conditions.

It is important to recognize that for absorption spectroscopy can also perturb the system it is measuring. In the above example, suppose two consecutive photons were incident on the atom. If the first was absorbed, the cross section for the second would be zero. This known as saturation and depends on the intensity of the photon field and the A coefficient

for the transition. Assuming that saturation is the intensity required to reduce the absorption cross section by half, then the intensity limit for a two-state system is,

$$I_s = \frac{2\sqrt{2}h\nu_0 A}{\lambda^2}, \tag{2.18}$$

where h is Planck's constant, and ν_0 is the nominal frequency of the transition.

CHAPTER 3

Experiment

3.1 Discharge Apparatus

The RPND apparatus used in the forthcoming experiments was similar in design to the coaxial geometry used by Vasilyak and others in their FIW studies [16]. It can be described as a cylindrical inner conductor, surrounded by a dielectric, covered by an outer conductor. In this case, the anode and the RPND served as the inner conductor. The dielectric was provided by a glass tube and an air gap. Finally, the outer conductor was a series electrically connected metal shells which served as the current return path. The geometry and its electrical equivalent are sketched in figure 3.1. Following from right to left, the inner conductor was composed of a vacuum window, a nipple, a double-sided flange tapped for an NPT connection, and the discharge tube containing the RPND. Unless otherwise noted, all vacuum components featured DN35 CF flanges with copper gaskets.

The tube was composed of borosilicate glass with metal vacuum flanges on both ends. The flanges of the tube also acted as the electrodes for the generation of the RPND. The glass tube had an inner diameter of 3.3 cm, an outer diameter of 4.0 cm, and a length of 22.9 cm. The overall length of the tube including the flanges was 30 cm. In the figure shown here, the right electrode served as the anode, and the left electrode was the cathode.

The dielectric surrounding the inner conductor was composed of several components. The vacuum window, nipple, double-sided flange, and anode were separated from the outer

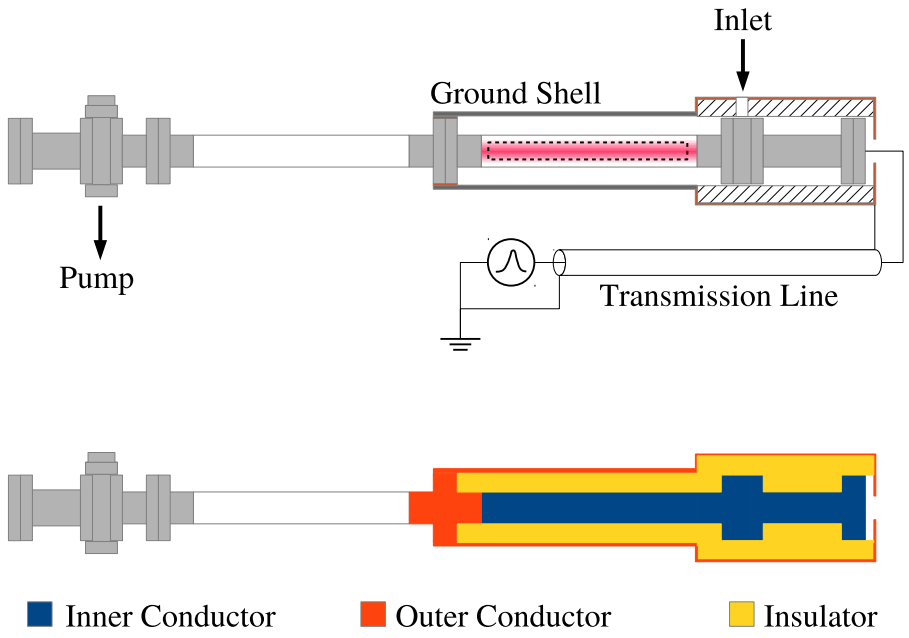

Figure 3.1: Two illustrations of the RPND apparatus. The upper version is an annotated sketch of the device, and the bottom version simplifies the geometry into its three electrical components.

conductor by an air gap and a polytetrafluoroethylene (PTFE) tube, 20 cm in length with an inner diameter of about 7.5 cm, and an outer diameter of 10 cm. The RPND portion of the inner conductor was separated from the outer conductor by the glass tube and an air gap of about 2.54 cm.

The left side of the discharge tube, or cathode, connected to the outer conductor and served as part of the current return path. Directly attached to the cathode was an alumninum tube, held in place by an acetyl resin shaft collar and a copper shim. Radial optical access to the discharge was provided by two slots milled into the ground shell. The slots were positioned on opposite sides of the shell and were 3.8 by 25.4 cm in length. The tube itself was 30 cm in length.

The end of the aluminum tube nearest the anode was affixed to a copper sheet which was oriented perpendicular with respect to the tube's axis of rotation. The sheet was 10 cm square, and was attached to the tube with conductive copper tape. A 5 cm diameter

hole was cut into the copper sheet to allow the discharge tube to pass through it. The sheet was secured to the edge of the PTFE tube by nylon screws. Surrounding the PTFE tube was a second shell, made of rolled copper sheet. This was electrically connected to the aluminum tube by a braided copper strap. The right end of the PTFE tube was covered by a second copper sheet, 10 cm square. Again, the sheet was secured to the PTFE tube by nylon screws and in electrical contact with the copper shell. In the center of the copper sheet was a HN bulkhead adapter for connection to the transmission line. The inner conductor of the bulkhead adapter was connected by a straight run of 5 cm of silicone-coated wire to the vacuum window flange. The outer conductor of the bulkhead adapter provided the ground connection for the discharge apparatus.[1]

The voltage pulse was generated by a FID power supply, supplied by ANVS, Inc. (model PT510NM). The amplitude of each pulse was fixed at 6.4 kV with a repetition rate of 1.0 kHz. Each pulse had a fixed width of 25 ns, with a 10%-90% rise time of approximately 4 ns and was roughly Gaussian in shape.A SRS DG645 delay generator was used to trigger the power supply output for all experiments and provided a reference time base for all measurements.

Preliminary experiments revealed multiple reflections between the power supply and the anode. A 13.7 m transmission line, made of RG213 coaxial cable, was used to temporally separate the reflections so that the effects of the individual pulses could be studied. The calculated delay introduced by the transmission line was 69.2 ns. As the reflection would have to cross the length of the transmission line twice before it reached the anode again, the total separation time between the initial pulse and each subsequent reflection was 138.4 ns. This calculated delay was found to be a close match in the measured delay.

A simplified version of the gas flow system can be seen in figure 3.2. The gas supply was provided by a bottle of ultra-high purity helium. Following the regulator, the helium passed through a digital flow controller which was set at 25.0 sccm for all experiments. The

[1]Measurements confirmed that the entirety of the outer conductor had a low DC impedance to ground. However, it is likely that at frequencies relevant to the RPND, the impedance is not negligible. As a result, the outer conductor likely floats to a finite voltage during operation.

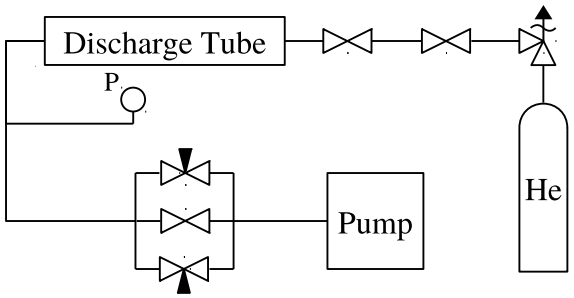

Figure 3.2: Simplified diagram of the gas flow path and pumping system.

helium then entered a gas distribution manifold, followed by a shutoff valve, a short run of 1/4" stainless steel tubing, another shutoff valve, about 2 m of 1/4" polyethylene tubing, and then the discharge tube via the double-sided flange.

The gas exited the discharge tube via an identical tube, on the side opposite the inlet, see figure 3.1. This second tube was intended to electrically isolate the discharge portion of the apparatus so that only a single conductive path to ground existed. The pressure was monitored downstream of the second tube with two capacitance manometers (one with a full scale range of 10 Torr, the other with a range of 100). Following that, the second tube was connected to an oil-seal roughing pump via three independent paths. The primary pump path had the highest gas conductance and was controlled by a bellows valve. However, this path was typically closed in favor of two needle valve bypasses. The needle valves were used to control the pumping speed and obtain the desired operating pressure. Immediately upstream of the roughing pump was a zeolite trap in order to limit oil backstreaming.

The base pressure of the system was measured to be approximately 15 mTorr. The leak rate was measured several times by evacuating the apparatus and then sealing it from the pump by all three pump paths. The leak rate was found to be 2.0×10^{-3} sccm. Given a constant flow rate of 25.0 sccm, the fractional impurity can be conservatively estimated to be 80 ppm.

The assembled discharge apparatus can be seen in figure 3.3. The RPND apparatus was supported two 1.5 in mounting posts with angle brackets. The mounting posts attached to a

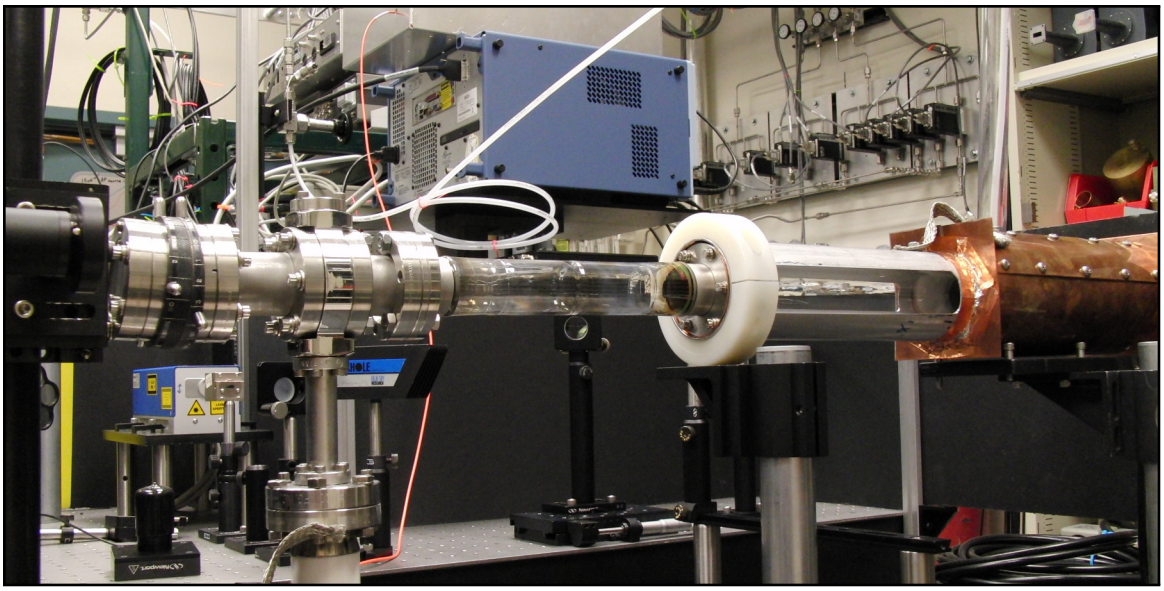

Figure 3.3: Photograph of the discharge apparatus.

4 ft by 2.5 ft optical breadboard, supported by urethane shock absorbers, and a rigid frame. The roughing pump was attached to the apparatus with flanged bellows in order to reduce mechanical vibrations.

All electrical measurements were made with a LeCroy 6100A WaveRunner oscilloscope which had a bandwidth of 1.0 GHz. Electrical connections to the oscilloscope were made with RG 50/U coaxial cable and standard BNC connectors. All connections were terminated at 50 Ω unless otherwise noted. The voltage of the pulses was monitored from a 1 : 1000 divider built into the power supply. The current was measured from a current shunt which crossed a small electrical break in the outer conductor of the transmission line. The shunt was built into the transmission line as close as possible to the power supply, about 3 cm from the output connector.

The current shunt was composed of nine, low inductance, 1.0Ω resistors connected in parallel. As illustrated in figure 3.4 the resistors were soldered to two strips of copper foil. This assembly was then wrapped around the electrical break in the transmission line, bridging it. Two short lengths of No. 18 copper wire were soldered to each side of the shunt assembly. These were then attached to a BNC bulkhead connector, fitted to a metal project

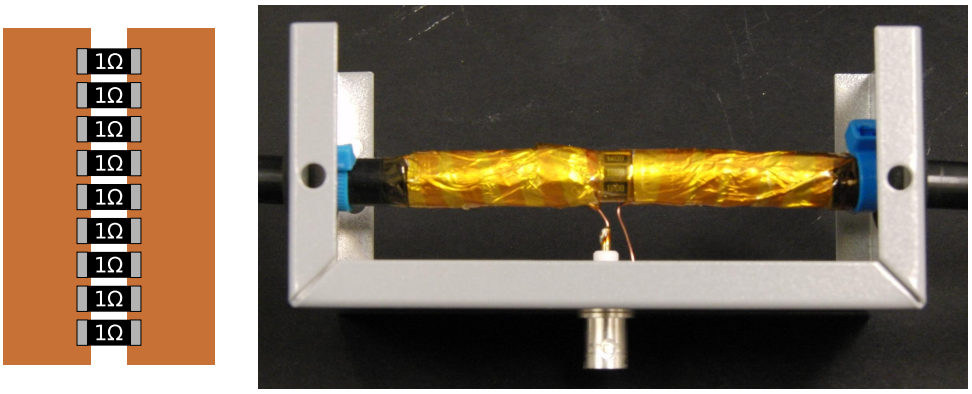

Figure 3.4: Sketch of the unassembled back-current shunt, and a photograph of it assembled around the transmission line.

box. The voltage across the resistors was used to measure the current traveling through the outer conductor of the transmission line. The copper foil was then secured to the outer conductor with several wraps of aluminum foil, followed by a layer of polyimide tape.

Data were retrieved from the oscilloscope with a desktop computer via the GPIB interface. Instrument control, data acquisition, and data storage were all managed by a LabView program. Analog input and output was handled with the auxiliary input and output ports of a SRS SR850 DSP lock-in amplifier.

3.2 Field Calculations

The electric field characteristics of the discharge apparatus were analyzed using Ansoft Maxwell 9, a two-dimensional, electrostatic solver. At the top of figure 3.5 is a logarithmic heat map of the electric field magnitudes within the device. Overlaid are the electric field vectors in magenta. Below this is a plot of the electric field on a linear scale, across the central axis of the apparatus and along the outer edge, adjacent to the glass tube. It is apparent that the field strength is the strongest at the triple point which occurs near the glass-metal seal. Also noticeable is the fast fall off of the electric field with distance from the anode. The presence of the external ground shield produces an electric field contour vastly different from that of two parallel plates. This is also reflected in the electric field vectors. Specifi-

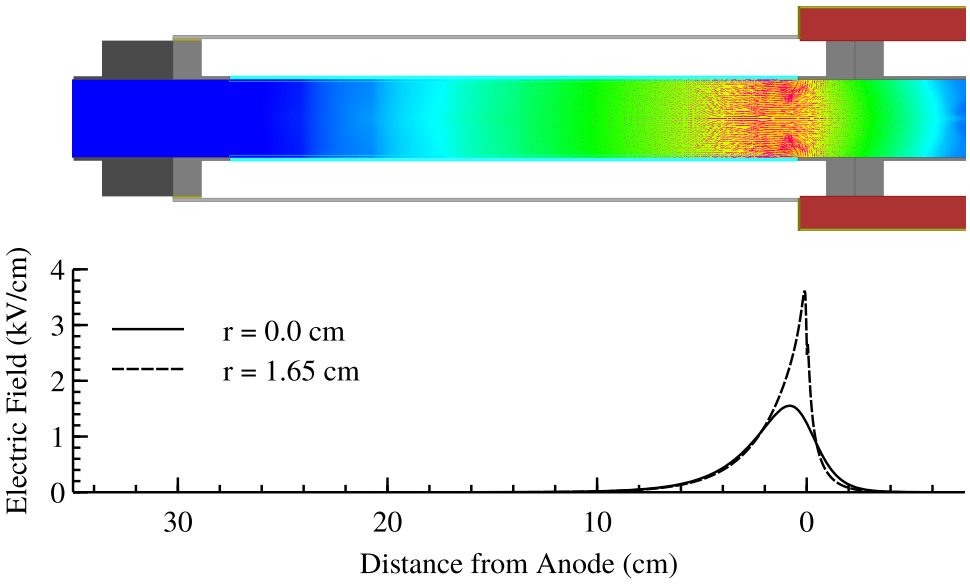

Figure 3.5: Heat map and vector plot of the electric field in the RPND discharge apparatus.

cally, the many locations possess fields with strong radial components, especially those near the anode.

These characteristics should result in a discharge that is somewhat different than the one-dimensional description of a streamer in chapter 2. First, assume that the electrons are distributed uniformly throughout the discharge tube, prior to the pulse. As a pulse is applied, ionization would preferentially take place near the anode. As the electrons would be drawn toward the anode, and leave behind some amount of positive space charge. However, as the positive space charge builds up, it would begin to act as a virtual anode, increasing the electric field further from the physical anode. The virtual anode would then begin to draw its own electron current, predominantly from around the edges, near the wall. In this manner, the discharge would propagate away from the anode, leaving a quasineutral ionized gas in the center of the discharge tube and a positive space charge region along the wall.

3.3 Operating Procedures

One of two operating procedures for the RPND was used depending on how recently the discharge had last been turned on. If it had been greater than one hour, a full startup procedure was used. Otherwise, an abbreviated process was used.

In the case that the discharge had not been operated for over an hour, the roughing pump was turned on and the primary pump path valve was opened as was the first shutoff valve upstream of the discharge chamber, seen in figure 3.2. The system was then allowed to pump down to its base pressure. Afterward the second upstream shutoff valve was opened and the system was again allowed to reach base pressure. At this point the helium flow was turned on and set to 25.0 sccm. The primary pump path was then closed and the needle valve bypasses were used to adjust the system pressure to 3.0 Torr.

Next, the delay generator was turned on and the output for triggering the power supply was activated. Then, the FID power supply was turned on. This would produce an easily visible discharge within the discharge tube. The system was allowed to operate at this condition for one hour in order to remove potential contamination on the walls and electrodes. At the end of this period, the voltage waveform was checked to ensure that it was consistent with previous experiments. Once this was confirmed, the pressure was adjusted to the desired operating condition.

The discharge was shutdown by first shutting off the power supply, followed by the delay generator. Then, the helium flow was shut off, and the primary pump path was opened. The system was allowed to come to base pressure before the two upstream shutoff valves were closed, after which the primary pump path was closed. The roughing pump was then shut off.

In the cases that the discharge had been operated within the last hour, it was possible to use an abbreviated startup procedure. This process was fundamentally the same as the previous one, however the discharge only required five minutes to reach a steady state. This was verified with multiple measurements of the current and voltage characteristics as well as

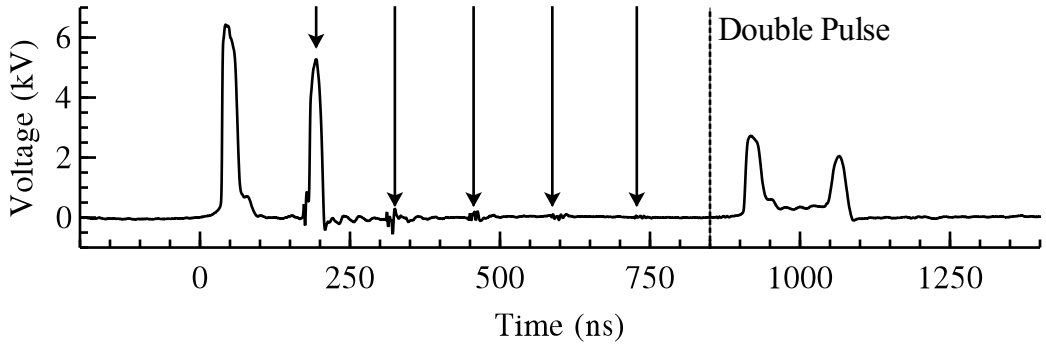

Figure 3.6: Typical voltage waveform of the RPND. Arrows indicate reflections back to the power supply. The dotted line delineates the time at which the power supply begins to exhibit double pulsing.

the discharge emissions. At times prior to this five minute equilibration period, the reflected pulse energy was noticeably higher, and the delay between the trigger pulse and the output pulse was variable.

3.4 Electrical Characteristics

The typical voltage waveform, as seen in figure 3.6, exhibited a number of features. It begins with an incident pulse at $t = 0.0$. 138 ns later, it is followed by the pulse that has been reflected from the anode. The reflected pulse is somewhat smaller, proportional to the energy deposited in the discharge. Additional reflections are visible at integer multiples of 138 ns. These subsequent reflections are much smaller than the initial one, suggesting that much of the remaining pulse energy was dissipated after the first reflection reached the anode. Curiously, a second pulse appears at 800 ns. This is believed to be a peculiarity of the power supply. For the most part, analysis of the RPND will focus on the times which precede 280 ns (the incident pulse and first reflected pulse).

The properties of the RPND were examined at: 0.3, 0.5, 1.0, 2.0, 3.0, 4.0, 8.0, and 16.0 Torr. The appearance of the discharge varied with the pressure in a continuous fashion, however it was apparent that there were three regimes of operation. At the low pressures,

0.3 and 0.5, it was difficult to initiate the discharge. Often, it would be necessary to increase the pressure to initiate the discharge, and then reduce the pressure to the desired conditions. The discharge appeared dim and relatively constricted about the central axis of the discharge tube, with a radial extent of approximately 1 cm. Accompanying these pressures was a large degree of electronic noise. This manifested primarily in the current waveforms, as seen in figure 3.7, as well as a number of equipment malfunctions.

As the pressure was increased (from 1.0-4.0 Torr), the electrical noise began to subside. The current waveforms in showed significant reductions in the ringing that was particularly prominent at lower pressures. In addition, the visual extent of the discharge increased substantially, to the point where it could be considered volume-filling. The discharge also increased its axial extent as well, eventually reaching well past its intended limit at the cathode. This occurred despite attempts to isolate the downstream pump sections from the discharge. It is possible to attribute this to the relatively large surface area of the anode in comparison to the cathode.

The discharge receded back to the intended cathode structure at the higher operating pressures, 8.0 and 16.0 Torr. This was accompanied by a decrease in the apparent brightness of the discharge to levels similar to that of the low pressure conditions. In contrast, the discharge appeared to remain volume-filling. While discharge initiation was difficult at the higher pressures, it was not accompanied by the electrical noise observed at lower pressures.

3.5 Energy Coupling

The product of the voltage and current waveforms, as seen in figure 3.7, gives the power deposited in the discharge as a function of time. Subsequently, the power integrated over time gives the total energy deposited in the discharge. However, this approach is somewhat complicated by several features of the RPND. As previously mentioned, the pulses produced by the power supply are not completely absorbed by the discharge. Therefore, the integration

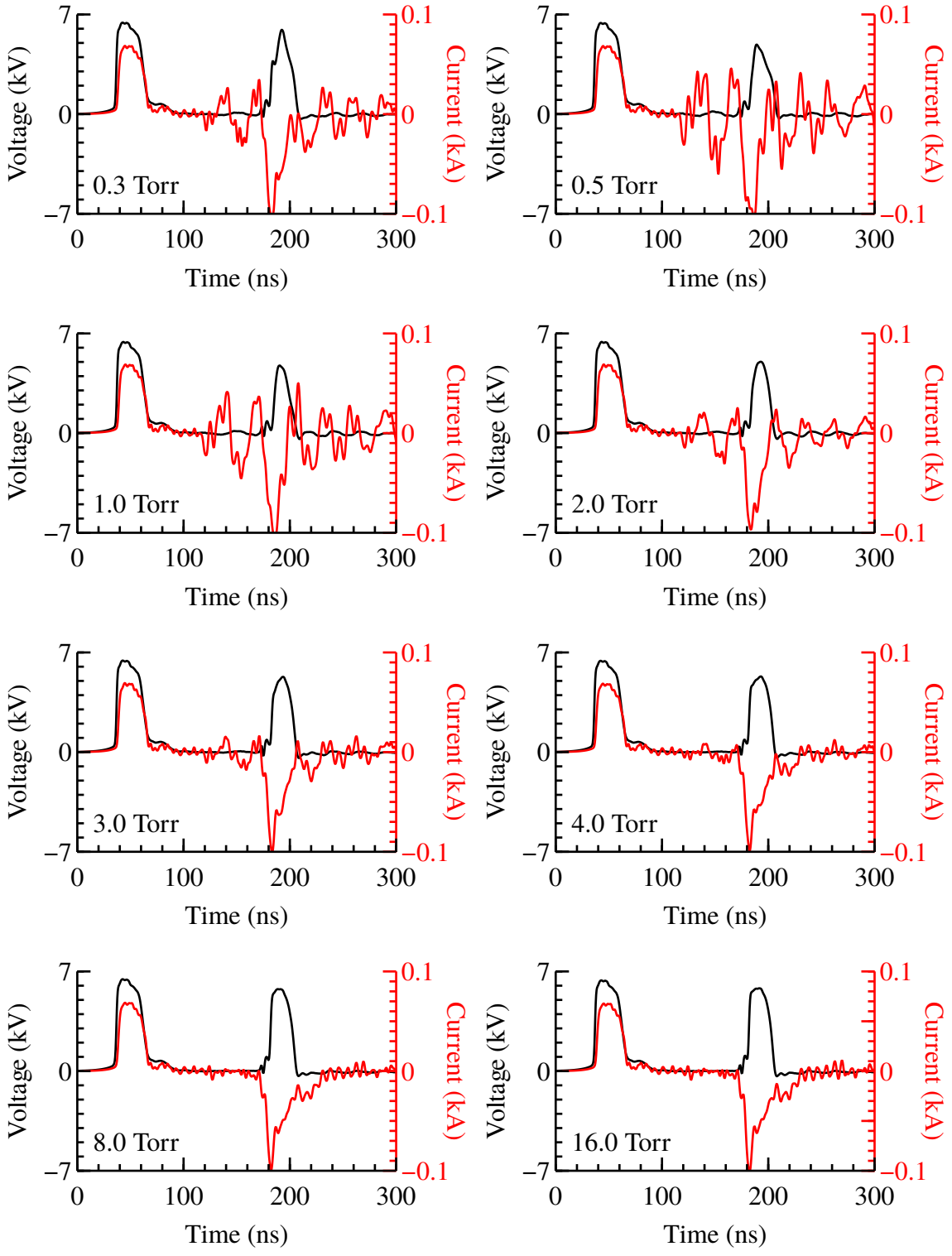

Figure 3.7: High resolution views of the voltage and current waveforms for the first incident and reflected pulse, at each of the operating pressures.

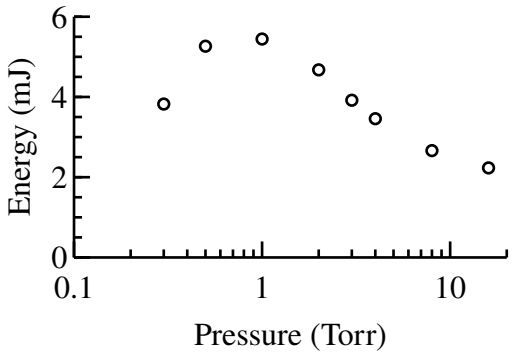

Figure 3.8: Plot of the energy coupled into the discharge with the first pulse as a function of pressure.

must be carried out over both the incident and the reflected pulse. Additionally, there is the concern that the oscillations in the current measurements could introduce fluctuations in the calculated energy deposition. However, the small voltage signal limits the error introduced by these fluctuations to less than 1%.

Figure 3.8 gives the total energy deposited for the first pulse at each of the operating conditions. The energy coupled to the discharge peaks at an energy of 5.5 mJ at a pressure of 1.0 Torr, after which it slowly decreases. This peak in the coupled energy is coincident with the peak brightness of the discharge. Together, these suggest that the density of excited states will be optimized at intermediate pressures.

Though there appear to be no direct comparisons available in the literature, several papers report on energy coupling for similar systems. Macheret, Schneider, and Murray studied a parallel plate RPND in air, at 1-10 Torr and reported a total energy deposition of 0.30-0.36 mJ, increasing with pressure [86]. Nishihara et al. recorded values of 1-2 mJ in a nitrogen RPND [79]. Pancheshnyi et al., in the study of an air-propane mixture at 750 Torr, found that each pulse deposited about 1.9 mJ of energy. Overall, the measured values for the deposited energy appear to be in comparable with those previously measured.

From an applications standpoint, the potential existence of a condition which optimizes the production of excited states is an interesting one. This behavior is also compelling

from a physical standpoint as it suggests a phase change in the competition of two or more processes. Though this kind of competition is reminiscent of Paschen's law, the duration of the pulse is too short for appreciable ion drift to occur (an estimated maximum of 3 mm), therefore secondary electron emission is not important. These observations provide further impetus for a close examination of the RPND properties, particularly the excited state dynamics.

CHAPTER 4

Metastable Measurements

CHAPTER 5

Emission Measurements

CHAPTER 6

Modeling

CHAPTER 7

Conclusions

APPENDIX A

Millimeter-Wave Interferometry

APPENDIX B

Rotational Spectroscopy

Previous studies have found that ionization waves can induce fast gas heating in molecular gas systems [99]. Up to 40% of the input energy can be converted into translational energy through dissociation of oxygen and quenching or electronically excited nitrogen states. In combustion applications, this gas heating can play an important role in the combustion chemistry, flame holding, and ignition delay. Likewise, gas heating can impact material processing and ionization efficiency in other RPND applications. As such, it is important to develop reliable temperature diagnostics for RPNDs in molecular gases.

As early as 2001, researchers have proposed the use of a novel, hybrid engine design for use in supersonic and hypersonic flight [100]. Like an earlier program which advertised the use of a magnetohydrodynamic (MHD) accelerator for controlling the gas inlet of a scramjet [101]. Essentially, a hypersonic flow would be ionized by some external source, and used as the working fluid in a downstream MHD generator. The electrical power produced by this system could be used for onboard electronics and subsequent acceleration stages. The slowed flow could then be used with a traditional turbojet engine.

One of the primary difficulties in the development of this MHD energy bypass engine was the efficient ionization of the inlet flow. Originally, Macheret suggested the use of electron beams, carefully tuned to coincide with the peak in the ionization cross section. However, the use of electron beams in the ionization of high pressure gases is accompanied by a large number of technical issues, similar to those some excimer lasers. Therefore, in 2006,

Nishihara et al. proposed the use of an RPND to produce an “electron beam” in situ [79].

B.1 Experiment

B.2 Theory

Researchers at have proposed the use of a novel hybrid engine for supersonic and hypersonic flight [].

The measurement of rotational spectra has been used several

BIBLIOGRAPHY

[1] J J Thomson. *Notes on Recent Researches in Electricity and Magnetism*. Clarendon Press, Oxford, UK, 1893.

[2] J D Huba. *NRL Plasma Formulary*. Naval Research Laboratory, Washington, D.C., 2011.

[3] Charlotte E Moore and Paul W Merrill. Partial Grotrian Diagrams of Astrophysical Interest. Technical report, National Bureau of Standards, Washington, D.C., 1968.

[4] Plasma 2010 Committee, Plasma Science Committee, and National Research Council. *Plasma Science: Advancing Knowledge in the National Interest*. Number 2007. The National Academies Press, Washington, D.C., 2007.

[5] K. E. Greenberg and G. A. Hebner. Electric-field measurements in 13.56 MHz helium discharges. *Applied Physics Letters*, 63(24):3282, 1993.

[6] E.E. Kunhardt. Generation of large-volume, atmospheric-pressure, nonequilibrium plasmas. *IEEE Transactions on Plasma Science*, 28(1):189–200, 2000.

[7] K H Becker, U Kogelschatz, K H Schoenbach, and R J Barker. *Non-Equilibrium Air Plasmas at Atmospheric Pressure*. Institute of Physics Publishing, Bristol, UK, 2005.

[8] Shahid Rauf and Mark J. Kushner. Dynamics of a coplanar-electrode plasma display panel. II. Cell optimization. *Journal of Applied Physics*, 85(7):3470, 1999.

[9] Muhammad Arif Malik, Abdul Ghaffar, and Salman Akbar Malik. Water purification by electrical discharges. *Plasma Sources Science and Technology*, 10(1):82–91, February 2001.

[10] H Ayan, D Staack, G Fridman, A Gutsol, Y Mukhin, A Starikovskii, A Fridman, and G Friedman. Application of nanosecond-pulsed dielectric barrier discharge for biomedical treatment of topographically non-uniform surfaces. *Journal of Physics D: Applied Physics*, 42(12):125202, June 2009.

[11] Munetake Nishihara and Igor V. Adamovich. Numerical Simulation of a Crossed Pulser–Sustainer Discharge in Transverse Magnetic Field. *IEEE Transactions on Plasma Science*, 35(5):1312–1324, October 2007.

[12] Kostya (Ken) Ostrikov, Uros Cvelbar, and Anthony B Murphy. Plasma nanoscience: setting directions, tackling grand challenges. *Journal of Physics D: Applied Physics*, 44(17):174001, May 2011.

[13] Ulrich Kogelschatz. Dielectric-Barrier Discharges: Their History, Discharge Physics, and Industrial Applications. *Plasma Chemistry and Plasma Processing*, 23(1):1–46, 2003.

[14] F Iza and J Hopwood. Split-ring resonator microplasma: microwave model, plasma impedance and power efficiency. *Plasma Sources Science and Technology*, 14(2):397–406, May 2005.

[15] Igor V. Adamovich, Walter R. Lempert, Munetake Nishihara, J. William Rich, and Yurii G. Utkin. Repetitively Pulsed Nonequilibrium Plasmas for Magnetohydrodynamic Flow Control and Plasma-Assisted Combustion. *Journal of Propulsion and Power*, 24(6):1198–1215, November 2008.

[16] L M Vasilyak, S V Kostyuchenko, N N Kudryavtsev, and I V Filyugin. Fast ionisation waves under electrical breakdown conditions. *Physics-Uspekhi*, 37(3):247–268, March 1994.

[17] J. L. Walsh, J. J. Shi, and M. G. Kong. Submicrosecond pulsed atmospheric glow discharges sustained without dielectric barriers at kilohertz frequencies. *Applied Physics Letters*, 89(16):161505, 2006.

[18] S M Starikovskaia, a Yu Starikovskii, and D V Zatsepin. The development of a spatially uniform fast ionization wave in a large discharge volume. *Journal of Physics D: Applied Physics*, 31(9):1118–1125, May 1998.

[19] Lewi Tonks and Irving Langmuir. A General Theory of the Plasma of an Arc. *Physical Review*, 34(6):876–922, September 1929.

[20] André Anders. Tracking down the origin of arc plasma science-II. early continuous discharges. *IEEE Transactions on Plasma Science*, 31(5):1060–1069, October 2003.

[21] S M Starikovskaia, N B Anikin, S V Pancheshnyi, D V Zatsepin, and A Yu Starikovskii. Pulsed breakdown at high overvoltage: development, propagation and energy branching. *Plasma Sources Science and Technology*, 10(2):344–355, May 2001.

[22] Jeffrey I. Levatter and Shao-Chi Lin. Necessary conditions for the homogeneous formation of pulsed avalanche discharges at high gas pressures. *Journal of Applied Physics*, 51(1):210, 1980.

[23] V.M. Efanov, V.V. Karavaev, A.F. Kardo-Sysoev, and I.G. Tchashnikov. Fast ionization dynistor (FID)-a new semiconductor superpower closing switch. In *Digest of Technical Papers. 11th IEEE International Pulsed Power Conference (Cat. No.97CH36127)*, volume 2, pages 988–991. IEEE, 1997.

[24] L B Loeb. Ionizing Waves of Potential Gradient: Luminous pulses in electrical breakdown, with velocities a third that of light, have a common basis. *Science (New York, N.Y.)*, 148(3676):1417–26, June 1965.

[25] C. Wheatstone. Versuche, die Geschwindigkeit der Elektricität und die Dauer des elektrischen Lichts zu messen. *Annalen der Physik und Chemie*, 110(3):464–480, 1835.

[26] W. v. Zahn. Spectralröhren mit longitudinaler Durchsicht. *Annalen der Physik und Chemie*, 244(12):675–675, 1879.

[27] John James. Die Abraham-Lemoinesche Methode zur Messung sehr kleiner Zeitintervalle und ihre Anwendung zur Bestimmung der Richtung und Geschwindigkeit der Entladung in Entladungsröhren. *Annalen der Physik*, 320(15):954–987, 1904.

[28] R. Whiddington. The Discharge of Electricity through Vacuum Tubes. *Nature*, 116(2918):506–509, October 1925.

[29] J. Beams. The Time Interval Between the Appearance of Spectrum Lines in Spark and in Condensed Discharges. *Physical Review*, 28(3):475–480, September 1926.

[30] B. F. J. Schonland and H. Collens. Development of the Lightning Discharge. *Nature*, 132(3332):407–408, September 1933.

[31] a. M. Cravath and L. B. Loeb. The Mechanism of the High Velocity of Propagation of Lightning Discharges. *Physics*, 6(4):125, 1935.

[32] L. Snoddy, J. Beams, and J. Dietrich. The Propagation of Potential in Discharge Tubes. *Physical Review*, 50(5):469–471, September 1936.

[33] E. Flegler and H. Raether. Der elektrische Durchschlag in Gasen nach Untersuchungen mit der Nebelkammer. *Zeitschrift f r Physik*, 99(9-10):635–642, September 1936.

[34] Leonard B. Loeb and John M. Meek. The Mechanism of Spark Discharge in Air at Atmospheric Pressure. I. *Journal of Applied Physics*, 11(6):438, June 1940.

[35] Leonard B. Loeb and J. M. Meek. The Mechanism of Spark Discharge in Air at Atmospheric Pressure. II. *Journal of Applied Physics*, 11(7):459, 1940.

[36] J. Meek. A Theory of Spark Discharge. *Physical Review*, 57(8):722–728, April 1940.

[37] L. Fisher and B. Bedderson. Formative Time Lags of Spark Breakdown in Air in Uniform Fields at Low Overvoltages. *Physical Review*, 81(1):109–114, January 1951.

[38] G. Kachickas and L. Fisher. Formative Time Lags of Uniform Field Breakdown in N2. *Physical Review*, 88(4):878–883, November 1952.

[39] G. Kachickas and L. Fisher. Formative Time Lags of Uniform Field Breakdown in Argon. *Physical Review*, 91(4):775–779, August 1953.

[40] EE Kunhardt and Y Tzeng. Development of an electron avalanche and its transition into streamers. *Physical review. A*, 38(3):1410–1421, August 1988.

[41] I D Chalmers. The transient glow discharge in nitrogen and dry air. *Journal of Physics D: Applied Physics*, 4(8):1147–1151, August 1971.

[42] W Rogowski, E. Flegler, and R. Tamm. Über Wanderwelle und Durchschlag. *Archiv für Elektrotechnik*, 18(5):479–512, September 1927.

[43] K. Buss. Der Stufendurchschlag. *Archiv für Elektrotechnik*, 26(4):266–272, April 1932.

[44] T E Allibone and J M Meek. The Development of the Spark Discharge. II. *Proceedings of the Royal Society A: Mathematical, Physical and Engineering Sciences*, 169(937):246–268, December 1938.

[45] T. E. Allibone and J. M. Meek. The Development of the Spark Discharge. *Proceedings of the Royal Society A: Mathematical, Physical and Engineering Sciences*, 166(924):97–126, May 1938.

[46] T E Allibone. The Mechanism of a Long Spark. *Journal of the Institute of Electrical Engineers*, 82(497):513–521, 1938.

[47] C V Boys. Progressive Lightning. *Nature*, 118(2977):749–750, November 1926.

[48] T E Allibone. Development of the Spark Discharge. *Nature*, 161(4103):970–971, June 1948.

[49] R F Saxe and J M Meek. Development of Spark Discharges. *Nature*, 162(4111):263–264, August 1948.

[50] E Kunhardt and W Byszewski. Development of overvoltage breakdown at high gas pressure. *Physical Review A*, 21(6):2069–2077, June 1980.

[51] Yu. L. Stankevich and V. G. Kalinin. Fast Electrons and X-Ray Radiation during the Initial Stage of Growth of a Pulsed Spark Discharge in Air. *Soviet Physics Doklady*, 12, 1968.

[52] Gennadii A Mesyats, Yu I Bychkov, and V V Kremnev. Pulsed nanosecond electric discharges in gases. *Soviet Physics Uspekhi*, 15(3):282–297, March 1972.

[53] L P Babich, T. V. Loiko, and L. V. Tarasova. The physics of high-voltage nanosecond discharges in dense gases. *Radiophysics and Quantum Electronics*, 20(4):436–442, April 1977.

[54] Leonid P Babich, T V Loĭko, and V A Tsukerman. High-voltage nanosecond discharge in a dense gas at a high overvoltage with runaway electrons. *Soviet Physics Uspekhi*, 33(7):521–540, July 1990.

[55] C. a. Fenstermacher. Electron-Beam-Controlled Electrical Discharge as a Method of Pumping Large Volumes of CO2 Laser Media at High Pressure. *Applied Physics Letters*, 20(2):56, 1972.

[56] a. Jay Palmer. A physical model on the initiation of atmospheric-pressure glow discharges. *Applied Physics Letters*, 25(3):138, 1974.

[57] R O Hunter. Electron beam controlled switching. In *International Pulsed Power Conference*, pages IC8–1 –IC8–6, New York, NY, 1976. Institute of Electrical Engineers, Inc.

[58] B M Koval'chuk and G A Mesyats. Rapid cutoff of a high current in an electron-beam-excited discharge. *Soviet Technical Physics Letters*, 2(252), 1976.

[59] N B Anikin, S V Pancheshnyi, S M Starikovskaia, and A Yu Starikovskii. Breakdown development at high overvoltage: electric field, electronic level excitation and electron density. *Journal of Physics D: Applied Physics*, 31(7):826–833, April 1998.

[60] S.V. Pancheshnyi, S.M. Starikovskaia, and A.Yu. Starikovskii. Measurements of rate constants of the v =0) and v =0) deactivation by N2, O2, H2, CO and H2O molecules in afterglow of the nanosecond discharge. *Chemical Physics Letters*, 294(6):523–527, September 1998.

[61] S V Pancheshnyi, S M Starikovskaia, and A Yu Starikovskii. Population of nitrogen molecule electron states and structure of the fast ionization wave. *Journal of Physics D: Applied Physics*, 32(17):2219–2227, September 1999.

[62] S M Starikovskaia. Plasma assisted ignition and combustion. *Journal of Physics D: Applied Physics*, 39(16):R265–R299, August 2006.

[63] S.O. Macheret, M.N. Shneider, and R.B. Miles. Modeling of air plasma generation by repetitive high-voltage nanosecond pulses. *IEEE Transactions on Plasma Science*, 30(3):1301–1314, June 2002.

[64] Igor V. Adamovich, Munetake Nishihara, Inchul Choi, Mruthunjaya Uddi, and Walter R Lempert. Energy coupling to the plasma in repetitive nanosecond pulse discharges. *Physics of Plasmas*, 16(11):113505, 2009.

[65] Dmitry S. Nikandrov, Lev D. Tsendin, Vladimir I. Kolobov, and Robert R. Arslanbekov. Theory of Pulsed Breakdown of Dense Gases and Optimization of the Voltage Waveform. *IEEE Transactions on Plasma Science*, 36(1):131–139, 2008.

[66] L D Tsendin and D S Nikandrov. An analytical approach to planar ionization fronts in dense gases. *Plasma Sources Science and Technology*, 18(3):035007, August 2009.

[67] Yvette Zuzeek, Inchul Choi, Mruthunjaya Uddi, Igor V. Adamovich, and Walter R Lempert. Pure rotational CARS thermometry studies of low-temperature oxidation kinetics in air and ethene–air nanosecond pulse discharge plasmas. *Journal of Physics D: Applied Physics*, 43(12):124001, March 2010.

[68] Osaka University) Ito, Tsuyohito (Frontier Research Base For Global Young Researchers, Osaka University) Kobayashi, Kazunobu (Center For Atomic And Molecular Technologies, Ruhr-University Bochum) Czarnetzki, Uwe (Institute For Plasma And Atomic Physics, and Osaka University) Hamaguchi, Satoshi (Center For Atomic And Molecular Technologies. Rapid formation of electric field profiles in repetitively pulsed high-voltage high-pressure nanosecond discharges. *Journal of Physics D: Applied Physics*, 43(6):062001, February 2010.

[69] Tsuyohito Ito, Kazunobu Kobayashi, Sarah Müller, Uwe Czarnetzki, and Satoshi Hamaguchi. Electric field measurements at near-atmospheric pressure by coherent Raman scattering of laser beams. *Journal of Physics: Conference Series*, 227:012018, May 2010.

[70] Brandon Weatherford, Edward Barnat, Zhongmin Xiong, and Mark Kushner. Two-Dimensional Electron and Metastable Density Profiles Produced in Helium Fast Ionization Wave Discharges. *Bulletin of the American Physical Society*, Volume 57,, October 2012.

[71] B B Slavin and P I Sopin. Breakdown of a neutral gas by ionizing waves of the gradient of a negative potential. *High Temperature1*, 30(1):1–9, 1992.

[72] S M Starikovskaia and A Yu Starikovskii. Numerical modelling of the electron energy distribution function in the electric field of a nanosecond pulsed discharge. *Journal of Physics D: Applied Physics*, 34(23):3391–3399, December 2001.

[73] Sergey V. Pancheshnyi, Deanna A. Lacoste, Anne Bourdon, and Christophe O. Laux. Ignition of Propane–Air Mixtures by a Repetitively Pulsed Nanosecond Discharge. *IEEE Transactions on Plasma Science*, 34(6):2478–2487, December 2006.

[74] Steven J Schneider, Hani Kamhawi, and Isaiah M Blankson. Efficient Ionization Investigation for Flow Control and Energy Extraction. *AIAA 47th Aerospace Sciences Meeting*, 2009.

[75] A Yu Starikovskii, A A Nikipelov, M M Nudnova, and D V Roupassov. SDBD plasma actuator with nanosecond pulse-periodic discharge. *Plasma Sources Science and Technology*, 18(3):034015, August 2009.

[76] J L Zimmermann, T Shimizu, H-U Schmidt, Y-F Li, G E Morfill, and G Isbary. Test for bacterial resistance build-up against plasma treatment. *New Journal of Physics*, 14(7):073037, July 2012.

[77] John E. Foster, Grigory Adamovsky, Sarah Nowak Gucker, and Isaiah M. Blankson. A Comparative Study of the Time-Resolved Decomposition of Methylene Blue Dye Under the Action of a Nanosecond Repetitively Pulsed DBD Plasma Jet Using Liquid Chromatography and Spectrophotometry. *IEEE Transactions on Plasma Science*, 41(3):503–512, March 2013.

[78] Guillaume Pilla, David Galley, Deanna a. Lacoste, Franois Lacas, Denis Veynante, and Christophe O. Laux. Stabilization of a Turbulent Premixed Flame Using a Nanosecond Repetitively Pulsed Plasma. *IEEE Transactions on Plasma Science*, 34(6):2471–2477, December 2006.

[79] Munetake Nishihara, J. William Rich, Walter R Lempert, Igor V. Adamovich, and Sivaram Gogineni. Low-temperature M=3 flow deceleration by Lorentz force. *Physics of Fluids*, 18(8):086101, 2006.

[80] Ainan Bao, Yurii G. Utkin, Saurabh Keshav, Guofeng Lou, and Igor V. Adamovich. Ignition of Ethylene–Air and Methane–Air Flows by Low-Temperature Repetitively Pulsed Nanosecond Discharge Plasma. *IEEE Transactions on Plasma Science*, 35(6):1628–1638, December 2007.

[81] Guofeng Lou, Ainan Bao, Munetake Nishihara, Saurabh Keshav, Yurii G Utkin, J William Rich, Walter R Lempert, and Igor V. Adamovich. Ignition of premixed hydrocarbon–air flows by repetitively pulsed, nanosecond pulse duration plasma. *Proceedings of the Combustion Institute*, 31(2):3327–3334, January 2007.

[82] David Z Pai, Gabi D Stancu, Deanna a Lacoste, and Christophe O Laux. Nanosecond repetitively pulsed discharges in air at atmospheric pressure—the glow regime. *Plasma Sources Science and Technology*, 18(4):045030, November 2009.

[83] Munetake Nishihara, Keisuke Udagawa Takashima, John R. Bruzzese, Igor V. Adamovich, and Datta Gaitonde. Experimental and Computational Studies of Low-Temperature Mach 4 Flow Control by Lorentz Force. *Journal of Propulsion and Power*, 27(2):467–476, March 2011.

[84] Tsuyohito Ito, Dirk Luggenhölscher, Kazunobu Kobayashi, Sarah Müller, Uwe Czarnetzki, and Satoshi Hamaguchi. Electric field measurement in an atmospheric or higher pressure gas by coherent Raman scattering of nitrogen. *Journal of Physics D: Applied Physics*, 42(9):092003, May 2009.

[85] Sarah Müller, Dirk Luggenhölscher, and Uwe Czarnetzki. Ignition of a nanosecond-pulsed near atmospheric pressure discharge in a narrow gap. *Journal of Physics D: Applied Physics*, 44(16):165202, April 2011.

[86] S. O. Macheret, M. N. Shneider, and R. C. Murray. Ionization in strong electric fields and dynamics of nanosecond-pulse plasmas. *Physics of Plasmas*, 13(2):023502, 2006.

[87] M. Laroussi and X. Lu. Room-temperature atmospheric pressure plasma plume for biomedical applications. *Applied Physics Letters*, 87(11):113902, 2005.

[88] XinPei Lu and Mounir Laroussi. Dynamics of an atmospheric pressure plasma plume generated by submicrosecond voltage pulses. *Journal of Applied Physics*, 100(6):063302, 2006.

[89] J L Walsh, D X Liu, F Iza, M Z Rong, and M G Kong. Contrasting characteristics of sub-microsecond pulsed atmospheric air and atmospheric pressure helium–oxygen glow discharges. *Journal of Physics D: Applied Physics*, 43(3):032001, January 2010.

[90] G V Naidis. Modelling of streamer propagation in atmospheric-pressure helium plasma jets. *Journal of Physics D: Applied Physics*, 43(40):402001, October 2010.

[91] Doug Breden, Kenji Miki, and Laxminarayan L. Raja. Computational study of cold atmospheric nanosecond pulsed helium plasma jet in air. *Applied Physics Letters*, 99(11):111501, 2011.

[92] Keisuke Takashima, Igor V. Adamovich, Zhongmin Xiong, Mark J. Kushner, Svetlana Starikovskaia, Uwe Czarnetzki, and Dirk Luggenhölscher. Experimental and modeling analysis of fast ionization wave discharge propagation in a rectangular geometry. *Physics of Plasmas*, 18(8):083505, 2011.

[93] Paul M. Bellan. *Fundamentals of Plasma Physics*. Cambridge University Press, 2008.

[94] M. J. Druyvesteyn and F. M. Penning. The Mechanism of Electrical Discharges in Gases of Low Pressure. *Reviews of Modern Physics*, 12(2):87–174, April 1940.

[95] Michael A. Lieberman and Allan J. Lichtenberg. *Principles of Plasma Discharges and Materials Processing*. John Wiley & Sons, Inc., Hoboken, NJ, USA, 2nd edition, April 2005.

[96] Francis F. Chen. *Introduction to plasma physics and controller fusion*. Springer, New York, NY, 2nd edition, 1984.

[97] A V Phelps. Compilation of Electron Cross Sections, 2002.

[98] A. E. Siegman. *Lasers*. University Science Books, Sausalito, CA, 1986.

[99] N a Popov. Fast gas heating in a nitrogen–oxygen discharge plasma: I. Kinetic mechanism. *Journal of Physics D: Applied Physics*, 44(28):285201, July 2011.

[100] Sergey O Macheret, Ronald J Lipinski, Richard B Miles, and Mikhail N Shneider. Electron-Beam-Generated Plasmas in Hypersonic Magnetohydrodynamic Channels. *AIAA Journal*, 39(6):1127–1138, June 2001.

[101] Evgeniy P Gurijanov and Phillip T Harsha. AJAX: New Directions in Hypersonic Technology. In *International Space Planes and Hypersonic Systems and Technologies*, pages 1–9, Seal Beach, CA, 1996. AIAA.